

C h a p t e r T h r e e

OBSERVED AND MODELED SHIFT OF CARBONATE-ASSOCIATED MICROBIAL
BIOMARKERS DURING *IN SITU* SIMULATED METHANE SEEP QUIESCENCE

David H. Case¹

in collaboration with,

Marcos Y. Yoshinaga², Alexis L. Pasulka¹, Katherine S. Dawson¹, Andreas J. Greve², Kai-Uwe
Hinrichs², and Victoria J. Orphan¹

¹Division of Geological and Planetary Sciences, California Institute of Technology, Pasadena,
CA, USA

²Organic Geochemistry Group, Department of Geosciences, University of Bremen, 28334
Bremen, Germany

This chapter is in preparation for publication.

3.0 ABSTRACT

Carbonate pavements at marine methane seeps preserve microbial signatures in the geologic record long after seep quiescence. However, the taphonomy of biomarkers associated with seep microorganisms is poorly understood. We characterized microbial intact polar lipid (IPL) profiles associated with carbonates from a well-studied methane seep ecosystem, Hydrate Ridge (OR, USA), and determined aspects of these profiles were well-differentiated by seepage activity and by mineralogy. We further contextualized IPL distributions with parallel interpretation of bacterial and archaeal 16S rRNA genes and core archaeal lipids. *In situ*, time-resolved transplant experiments simulated methane seep quiescence, enabling direct observation of shifts in biomarker profiles on short (13 month) timescales, as well as forward modeling of continued biomarker profile changes beyond 13 months.

Bulk IPL profiles exhibit less change than 16S rRNA gene biomarkers upon transplantation simulating seep quiescence. However, differences between IPL and core lipid profiles also indicate IPLs do not represent an integrative record of microorganisms with the longevity of core lipids. The majority of IPLs are cosmopolitan to all seep conditions, but the distribution of some IPLs are especially sensitive to seep activity (e.g., phosphatidylcholine-diacylglycerol-C34:2 [PC-DAG-C34:2]) and respond to quiescence of methane seepage on the order of years. Estimates of cell concentrations from total lipid amounts indicate populations of ANME-1 ($\sim 10^7$ to 10^8 cells/cm³) and ANME-2 ($\sim 10^7$ to 10^{10} cells/cm³) in carbonates from active seeps are similar to sediments from similar environments, emphasizing the likely importance of carbonate-associated anaerobic methanotrophs in seep methane cycling. Relative proportions of ANME-1 IPL biomarkers appear to be robust for determination of whether active vs low-activity seep conditions are recorded. Core lipids appear biased toward ANME-1 over ANME-2 probably a result of differential lipid degradation rates. Some bacterial IPLs likely associated with sulfate-reducing deltabacteria exhibit a closer association with dolomite than calcite mineralogy. An

integrated understanding of microbial biomarker distribution and time-dependent behavior is critical for accurate interpretations of paleo-seep carbonates.

3.1 INTRODUCTION

The central microbial metabolism in marine methane seeps is the sulfate-coupled anaerobic oxidation of methane (AOM) which is estimated to consume >80% of contemporary subsurface methane, thereby preventing its release into the ocean/atmosphere system (Reeburgh 2007). Marine methane seeps have been proposed to play many roles throughout Earth history. These have included implications for the ancient evolution of life (Rasmussen 2000; Peckmann and Goedert 2005), extreme warming events such as the Paleocene-Eocene Thermal Maximum (Katz et al. 1999) or Neoproterozoic post-glacial warm periods (Jiang et al. 2003), and/or perturbations in Earth's carbon cycle (Hinrichs 2002; Schrag et al. 2013). Although these hypotheses continue to be debated (Barstow et al. 2011; Slotznick and Fischer 2016), it is true that methane seeps have been pervasive for hundreds of millions of years (or longer) and during that time have likely played important roles in cycling Earth's carbon inventory.

Carbonate precipitates are ubiquitous features of the seafloor landscape at methane seeps (Suess et al. 1985; Moore et al. 1990; Boetius and Suess 2004). These precipitates, ranging in size scale from 10^{-3} to 10^2 meters, are hypothesized to form as a result of alkalinity generated during sulfate-coupled AOM (Berner 1980; Ritger et al. 1987). Carbon isotopes provide supporting evidence for this, with seep carbonates often exhibiting depleted $\delta^{13}\text{C}$ values diagnostic of methanotrophy (Kulm and Suess 1990; Gieskes et al. 2005). A variety of carbonate mineralogies have been observed in seep settings including aragonite, calcite, dolomite, and mixtures thereof (e.g., Naehr et al. 2007). It is hypothesized that dolomites form deep in the sediment column, below AOM zones, while aragonites form in sulfate-replete near-surface sediments and calcites precipitate at or near the zones of highest AOM (Burton 1993; Greinert et al. 2001; Naehr et al.

2007; Bayon et al. 2009; Blättler et al. 2015). In addition to their occurrence and distribution at or near the seabed, seep carbonates also extend many meters beneath the seafloor and effectively represent the dominant volumetric fraction of habitat substrate at methane seeps (Marlow et al. 2014a and references therein). The links between microbial activity and mineralogy are not well understood, but pore fluid geochemistry and flux, as well as microbial assemblage composition, have been identified as possible drivers of mineralogy (Aloisi et al. 2002; Teichert et al. 2005; Reitner et al. 2005; Stadnitskaia et al. 2008; Leefmann et al. 2008; Birgel et al. 2011; Hagemann et al. 2012).

Censuses of seep sediment-hosted microbial diversity based on the 16S rRNA gene have recently revealed a dominance of *Methanomicrobia*, *Deltaproteobacteria*, and candidate divisions Hyd24-12 and JS1 as compared to other marine environments (Pop Ristova et al. 2015; Ruff et al. 2015). However, 16S rRNA gene profiles in exhumed seep carbonates recovered from the seabed are distinct from those in seep sediments (Marlow et al. 2014b; Case et al. 2015). These carbonate-associated microbial assemblages are less dominated by Deltaproteobacterial and bacterial Candidate Division JS1 16S rRNA gene sequences than seep sediments and are characteristically rich in the uncultured gammaproteobacterial JTB255 Marine Benthic Group (Case et al. 2015). Carbonate-associated microbial assemblages, like those in seep sediments, appear to be strongly shaped by the magnitude of local seepage (Lloyd et al. 2010; Rossel et al. 2011; Case et al. 2015). Recent measurements of active AOM by carbonate-hosted microbial assemblages established that viable methanotrophic microorganisms inhabit seep carbonates (Marlow et al. 2014a). Furthermore, seep carbonate 16S rRNA gene diversity does not appear to record historically active microbial populations: microbial 16S rRNA gene biomarker richness decreases markedly upon imposed seep quiescence during *in situ* ecological transplant experiments and 16S rRNA gene profiles are distinct between active and low-activity seepage sites (Case et al. 2015).

The presence of microbial lipid biomarkers recovered from Phanerozoic carbonates, often highly depleted in $\delta^{13}\text{C}$, have been used to link geologic outcrops to historic methane seepage sites (Peckmann et al. 1999; Thiel et al. 1999; Peckmann et al. 2002; Goedert et al. 2003; Birgel et al. 2006b; a; Birgel et al. 2008b; a; Kiel et al. 2013; Natalicchio et al. 2015; Little et al. 2015). Some studies have further attempted to reconstruct the strength of past seepage conditions (Leefmann et al. 2008; Peckmann et al. 2009; Birgel et al. 2011; Hagemann et al. 2012) or microbial ecology from detailed analysis of recovered microbial lipids (e.g., ANME-1 vs ANME-2 ratios; Blumenberg et al. 2004; Birgel et al. 2006a; Niemann and Elvert 2008; Peckmann et al. 2009; Birgel et al. 2011; Natalicchio et al. 2015). However, the interpretation of lipid biomarkers in ancient carbonates as being representative of past biochemical and ecological environments is hampered by several factors. First, co-incorporation of lipids from carbonate-specific cells with lipids from exogenous sedimentary and planktonic cells (Peckmann et al. 2002; Hoffmann-Sell et al. 2011; Blumenberg et al. 2015) can expand and complicate the environmental signal recorded in lipid biomarkers. Similar results have been reported for marine glycerol-diphytanyl-glycerol-tetraether (GDGT) lipid profiles, where sedimentary and planktonic signals appear to be mixed (Pearson et al. 2016). Second, post-depositional thermal alteration and diagenesis can alter lipid profiles, thereby impacting interpretation of environmental conditions at the time of deposition (Goedert et al. 2003; Hagemann et al. 2012). A third process has remained relatively unexplored: genuine shifts in the seep-associated microbial assemblages after the period of seep activity but prior to incorporation into the geologic record. For example, ANME-1 archaea are often observed to predominate over ANME-2 in low fluid flux regimes (and vice versa in high flux seeps), and thus the recovery of ANME-1 vs ANME-2 lipids has been used to infer past seepage magnitude (Blumenberg et al. 2004; Stadnitskaia et al. 2008; Peckmann et al. 2009). However, if, during progressive seep quiescence, the carbonate-hosted microbial assemblage and associated biomarkers were to shift in reflection of the diminishing seepage flux as is observed in 16S rRNA

genes, the resulting recorded biomarker inventory would not fully represent the environmental history of methane seepage.

IPLs have generally been considered to degrade quickly after cell death due to the instability of the bond between the glycerol backbone and polar head group, leading to the assumption that IPLs reflect living biomass (White et al. 1979; 1997; Zink et al. 2003; Sturt et al. 2004). However, recent studies have called this into question. In one study, laboratory incubations of anoxic sandy North Sea sediments were amended with dead cells of the archaeon *Haloflex volcanii* and the eukaryote *Saccharomyces cerevisiae* (eukaryotic non-isoprenoidal ester-bound IPLs are structurally similar to those of bacteria). After 100 days, >75% of ester-bound IPLs had degraded, while no degradation was measured of the archaeal ether-bound IPLs (Logemann et al. 2011). A second study spiked a radioactive synthetic analog of a monoglycosidic archaeol (^{14}C -1G-AR) into North Sea and deep subsurface sediments, then measured IPL degradation over 300 days. The IPL degradation half-life was extrapolated to be ~3-300 ky, depending on environmental conditions (Xie et al. 2013). Finally, diglycosidic (2G) GDGTs were recently measured to have slow production rates and hypothesized to be synthesized by ANME-1 in stationary phase rather than active growth (Kellermann et al. 2016). The taphonomy of IPL biomarkers remains an active area of debate and is critical to understand for application in modern and/or ancient systems, particularly because IPLs (and core lipids) can be preserved in authigenic carbonate minerals.

Methane seepage itself is known to fluctuate on an extremely wide range of timescales, from diurnal (tidal forcing) to interglacial (changes in mean sea level), suggesting the activation and quiescence of seepage is a highly relevant process impacting microbial assemblages at methane seeps (Tryon et al. 1999; 2002; Teichert et al. 2003). A laboratory experiment with seep sediments from the North Sea, in which methane was supplied for 120 days, removed for 36 days, resupplied for 40 days, and then removed permanently, showed AOM to respond on the scale of days to varying methane flux (Wegener and Boetius 2009). However, the study only examined rates of AOM and not biomarkers of the constituent methanotrophic microbial consortia. Adding

further complexity, modeling and empirical measurements indicate individual carbonate pavements precipitate over timescales of 10^2 - 10^3 years, implying that a single carbonate can record periods spanning multiple cycles of seepage activation and quiescence in cases of rapidly shifting seep activity (Luff et al. 2004; Bayon et al. 2009). Understanding whether and to what extent carbonates record the extant microbial community structure vs an integrative record of all previously inhabiting microorganisms is therefore of critical importance. Furthermore, the history of microbial assemblages recorded in seep carbonates may vary depending on the type of biomarker analyzed (DNA vs IPL vs core lipid).

In this study we (i) describe the IPL profiles associated with modern seep carbonates at Hydrate Ridge, OR, USA, and link differences in IPL profiles to environmental factors, (ii) employ 13-month, ecological *in situ* transplantation experiments to test the impact of seep quiescence on lipid biomarker profiles, and (iii) forward model the response of both IPL and 16S rRNA gene biomarkers to extended conditions of quiescence, including comparison to archaeal core lipids from our sample set. Ultimately this enables hypothesis development regarding the changes in microbial community structure that occur when a seep becomes dormant – a phase in the seep life cycle common to carbonates which eventually enter the geologic record.

3.2 MATERIAL AND METHODS

3.2.1 FIELD EXPERIMENTS AND SAMPLE COLLECTION

All carbonate experiments and sample collections were conducted at Hydrate Ridge (HR), a well-studied natural laboratory of methane seepage offshore OR, USA (Suess et al. 1985; Tryon et al. 1999; Boetius et al. 2000; Sahling et al. 2002; Tryon et al. 2002; Treude et al. 2003; Boetius and Suess 2004; Gieskes et al. 2005; Levin et al. 2010; Pasulka et al. 2015; Case et al. 2015; Table 1). Twenty-two of our 23 samples were collected from a site referred to as Hydrate

Ridge North (HR-N), a promontory at ~600 meters below sea level (mbsl) just above the oxygen minimum zone (~0.7 mL L⁻¹ O₂; Levin et al. 2010). One sample was recovered from a deeper promontory (775 mbsl) demonstrating active seepage located approximately 12 km farther south (HR-S) and bathed in oxygen-depleted waters (0.2-0.3 mL L⁻¹ O₂; Levin et al. 2010). Specific sampling stations (e.g., “HR-3”; see Case et al. 2015 for coordinates) were identified as active (HR-3 and HR-7) or low-activity (HR-4 and HR-8) based on the presence or absence, respectively, of diagnostic seafloor characteristics such as methane ebullition and/or chemosynthetic communities such as mats and clam beds (as described in Orphan et al. 2004). Later pore water measurements confirmed that active stations exhibit higher sulfide concentrations than low-activity stations, corroborating our activity designations (Pasulka et al. 2015). High throughput Illumina sequences of the 16S rRNA gene V4 region for all 23 samples have recently been published in a study of seep microbial 16S rRNA gene diversity (Case et al. 2015).

The 23 seep carbonates were assigned to one of three categories: native, transplantation, or colonization (following designations in Case et al. 2015). Native carbonates were exhumed carbonate slabs and blocks recovered directly from the seafloor and provide essential context for interpreting the biomarker signatures in the transplantation and colonization experiments in active and low-activity sites. Transplantation carbonates were transferred from the same stations as native carbonates via the DSV *Alvin* from active to low-activity stations, and vice versa (paired active and low-activity stations were separated by 10¹-10² meters on the seafloor). These replicated experiments simulated rapid seep quiescence (active to low-activity) and seep activation (low-activity to active). The transplanted samples were incubated for 13 months on the seafloor before recovery. Colonization carbonates represent samples of a large dolomitic and calcitic carbonate slab that had been collected from a seep site during a previous cruise and subsequently sterilized by autoclaving in the lab prior to deployment as part of this study. The colonization carbonates were placed on the seafloor for 13 months at the same stations as the transplantation

experiments. All collection and experimentation was conducted during R/V *Atlantis* cruises AT15-68 (2010) and AT18-10 (2011). Upon recovery onboard ship, all carbonates were processed into subsamples and frozen at -80°C for subsequent DNA and lipid biomarker analysis.

3.2.2 BIOMARKER EXTRACTION AND QUANTIFICATION

Two independent lipid datasets were generated: a quantitative IPL dataset that included both bacterial and archaeal lipids (hereafter “IPL dataset”), and a semi-quantitative dataset exclusive to Archaea which consisted of both intact polar and core lipids (hereafter “archaeal semiquantitative lipids dataset” or “ASL dataset”; relative abundance values within this dataset are robust, but not absolute core lipid concentrations). To prepare samples for total lipid extraction, subsamples of frozen carbonates were lyophilized overnight (~10-30 g/sample), followed by pulverization for 4 minutes in a tungsten-carbide shatter box. The box was cleaned thoroughly with isopropyl alcohol between samples to remove debris. Powders were then extracted as total lipid extracts (TLEs) using a modified Bligh and Dyer protocol (Sturt et al. 2004), after adding an internal standard (phosphatidylcholine C_{21:0}/C_{21:0}). The obtained TLEs were characterized by high-performance liquid chromatography mass spectrometry (HPLC-MS). TLEs were measured in positive ionization mode, while scanning a mass-to-charge (m/z) range of 150–2,000, with automated data-dependent MS/MS fragmentation of base peak ions. Compound detection was conducted on a Bruker maXis Ultra-High Resolution qToF-MS, equipped with an electrospray ionization (ESI) interface. For quantitative IPL analysis, separation of polar lipids was achieved on a Dionex Ultimate 3000 UHPLC equipped with a Waters Acquity UPLC BEH Amide column (150 x 2.1 mm, 1.8 μm particle size), operating in normal phase. Rings and unsaturation patterns of archaeal tetraether lipids were evaluated by reverse phase chromatography with a Waters Acquity BEH C₁₈ column. Details of the chromatographic conditions and analyses are described in Wörmer et al. 2013). Compound identification was

achieved by monitoring exact masses of possible parent ions (present mainly as H^+ and NH_4^+ adducts) in combination with characteristic fragmentation patterns (Sturt et al. 2004; Yoshinaga et al. 2011). The reported concentrations of microbial lipids are based on the peak areas of molecular ions, accounting for potential differences in ionization during HPLC-MS routines. A list of commercially available and purified standards used to determine the response factors of polar lipids are provided in the Supplementary Material (Table S1). It is worth mentioning that carbonate samples were additionally extracted using HCl (e.g. Birgel et al. 2006b) and analyzed for comparison with the Bligh and Dyer method. Similar or even higher yields for both polar lipids and archaeal core lipids were obtained using the Bligh and Dyer method relative to the HCl treatment (data not shown).

3.2.3 MINERALOGICAL AND ISOTOPIC CHARACTERIZATION

All samples were subjected to bulk mineralogical and carbon isotopic analysis. Carbonates were first ground in sterile ceramic mortar and pestle to generate a homogenous powder. Mineralogy was then determined by X-ray diffraction (XRD) on a Phillips X'Pert Multi Purpose instrument. Measurements were taken from 10° to 70° 2θ with step size of 0.05° . SiO_2 standards were run to confirm peak location accuracy. Similar to previous studies, areas of diagnostic peaks for aragonite ($2\theta = 26.3^\circ$), calcite ($2\theta = 29.5^\circ$), and dolomite ($2\theta = 31.0^\circ$) were used to determine quantitative mixing ratios of bulk mineralogy for each rock (Tennant and Berger 1957; Bergmann 2013; Marlow et al. 2014b; Table 1). Ultimately, the carbonates were coarsely divided into two categories – aragonitic and calcitic/dolomitic (Supplemental Text).

Bulk organic carbon isotopic composition, as well as weight percent organic carbon, was determined for each carbonate. Organic carbon was isolated by digesting ~ 4 mg bulk powder in 2N H_3PO_4 three times. All samples were analyzed via continuous flow (He; 100 mL/min) on a Costech Instruments Elemental Combustion System model 4010 (EA) by oxidation at $980^\circ C$ over

chromium (III) oxide and silvered cobalt (II, III) oxide followed by reduction over elemental copper at 650 °C. CO₂ was subsequently passed through a water trap and then a 5 Å molecular sieve GC at 50 °C to separate N₂ from CO₂. CO₂ was diluted with helium in a Conflo IV interface/open split prior to analysis. δ¹³C values were measured on a Thermo Scientific Delta V Plus IR-MS. δ¹³C values were corrected for sample size dependency and then normalized to the VPDB scale with a two-point calibration and internal standards.

3.2.4 STATISTICAL ANALYSIS

Biomarker “richness”, a measure of ecological alpha diversity (i.e., within-sample diversity) was defined as a simple presence/absence count of the total lipids (or 16S rRNA gene OTUs) present in a given sample, regardless of the biomarkers’ relative abundance. Bray-Curtis similarity, a measure of ecological beta diversity (i.e., between-sample diversity), was calculated as the similarity of total biomarker profiles (incorporating not only presence but also abundance of biomarkers) between samples. This was done by two methods: first, Bray-Curtis similarities were calculated based on the raw quantitative IPL data (in ng/g). Second, Bray-Curtis similarities were calculated on IPL data which had previously been transformed into relative abundance. Then, for both calculation methods, nonmetric multidimensional scaling (NMDS) ordinations and Analysis of Similarity (ANOSIM) tests were computed in R using the ‘vegan’ package v2.0-10 (Oksanen et al. 2013; R Core Team 2014). NMDS ordinations were computed with the ‘metaMDS’ function on a Bray-Curtis similarity matrix (distance=“bray”) set to two dimensions (k=2), with a maximum of 100 iterations (trymax=100) and the ‘monoMDS’ engine. ANOSIM calculations were also executed on a Bray-Curtis similarity matrix with a maximum of 999 permutations. Each lipid from both the relative abundance IPL and archaeal ASL datasets was tested for correlation against each OTU from the iTag 16S rRNA gene dataset using the ‘cor’ function in R (method=“pearson”), with p-values calculated using the ‘cor.test’ function (method=“pearson”).

3.2.5 MODELING TIME-DEPENDENT BIOMARKER PROFILE SHIFTS

We took two modeling approaches in interpreting our time-resolved transplantation experiments. First, carbonate-associated biomarker richness (the presence/absence of biomarkers and the degree to which they are detected across multiple sample types) was used to track and forward model whole-community microbial responses to seep quiescence. Second, we examined variations in concentration of individual IPL and 16S rRNA gene biomarkers which, based on our dataset, may be diagnostic of active or low-activity methane seep environments.

Because richness is highly sensitive to sampling depth (discovery opportunity), the richness analyses were restricted to an equal number of samples per category examined. For example, Fig. 5 was limited to two samples per category because of the low sample number of our transplant-to-low-activity experiments. Therefore, the results of our richness analyses (Fig. 5, 6) are technically only representative of the specific samples examined. However, we tested multiple permutations of samples and found similar results for the majority of sample combinations, such that the results presented in Fig. 5 and Fig. 6 are generally supported across the whole dataset (Supplemental Text).

We modeled total biomarker richness as a function of time (t) in carbonates during seep quiescence by the following general equation:

$$\text{Richness}(t) = a + b + c \quad (\text{Eq. 1})$$

where a is the constant richness never lost or gained (the cosmopolitan richness found in all samples; Table 2), b is the remaining active-type richness (a vector of decreasing richness with time; Table 2), and c is the richness gained from low-activity stations (a vector of increasing richness with time; Table 2; Supplemental Text). Our time-resolved transplantation data gives us three time points necessary to empirically derive an equation to fit the microbial community dynamics observed at Hydrate Ridge: $t=0$ years, the community structure of native-active carbonates prior to seep quiescence, $t=1.08$ years, the community structure after 13 months of

seep quiescence, and $t \gg 1.08$ years, the community structure expected when the microbial assemblage has fully turned over to low-activity-type conditions (Table 2; Supplemental Text).

We assume a log-linear response rate of microbial biomarkers over time, congruent with previous observations of microbial processes (Shade et al. 2013). Ecologically, a log-linear model implies the microbial communities are responding most rapidly during immediate onset of seep quiescence, with slower response over time. A rapid metabolic response of AOM-related microorganisms is supported by previous laboratory incubations (Wegener and Boetius 2009). Log-linear responses to environmental change are well-supported in the other biological systems as well (Benincà et al. 2008; Korhonen et al. 2010), although the availability of high-throughput next generation sequencing has only recently allowed microbial ecologists to begin fitting models to high resolution time series data (Faust et al. 2015). More experimental time points would be necessary in order to fully test and validate this assumption for microbial community responses at Hydrate Ridge. These models were built to match the experimental observation of an initial drop in biomarker richness upon quiescence and predict a gradual transition to the characteristic biomarker richness of the native-low-activity carbonates, although the models were not forced to recreate the input data points (Fig. 6c). We applied the modeling to our parallel 16S rRNA gene (Fig. 6b), IPL (Fig. 6c), and archaeal core lipid (Fig. 6d) datasets.

In our second modeling approach we examined our data to identify specific IPLs (and 16S rRNA gene OTUs) characteristic of active and low-activity seepage conditions and which could be useful biomarkers for future geobiological studies of seepage activity and AOM. In order to identify key IPL biomarkers of interest (using the quantitative IPL dataset), we applied three criteria to the entire suite of native-active, native-low-activity, and transplant-to-low-activity carbonates (Q1=first quartile; Q3=third quartile):

- (i) *This criterion ensures there is a significant difference in concentration of the IPL between active and low-activity seep conditions.*
 In order to qualify as an active-type IPL, Q1 of the IPL among the native-active carbonates must be greater than Q3 of the IPL among the native-low-activity carbonates. In order to qualify as a low-activity-type IPL, Q3 of the IPL among the native-active carbonates must be less than Q1 of the IPL among the native-low-activity carbonates.
- (ii) *This criterion ensures that upon seep quiescence the concentration of the IPL is changing in a manner consistent with the observed difference between active and low-activity conditions.*
 The median of the IPL among the transplanted (active to low-activity) carbonates must be between the medians of the IPL among the native-active and native-low-activity carbonates.
- (iii) *This criterion ensures that spurious IPL biomarkers are not identified with extremely low concentrations among the dataset.*
 In order to qualify as an active-type IPL, the median of the IPL among native-active carbonates must be greater than 4.43 ng/g in concentration. In order to qualify as a low-activity-type IPL, the median of the IPL among native-low-activity carbonates must be greater than 4.43 ng/g in concentration. For this criterion, the value of 4.43 ng/g was chosen because it is 1% of the median total IPL concentration for all native and transplantation carbonates in this study.

In order to identify key 16S rRNA genes of interest, we employed the same criteria with one modification on the third criterion in order to account for the relative abundance nature of the 16S rRNA gene dataset: rather than a cutoff value of 4.43 ng/g (irrelevant to the 16S rRNA gene data), we applied a cutoff of 1% relative abundance. After identifying specific biomarkers (Fig. 7), we applied a log-linear approach in order to generate biomarker-specific models (Fig. 8; Table 3).

3.3 RESULTS

The cumulative per-sample concentrations of 201 archaeal and bacterial IPLs ranged three orders of magnitude between 25 ng/g and 12,189 ng/g (Fig. 1a; Table 1; Table S2). Among active seep stations both aragonitic and calcitic/dolomitic-type carbonates were recovered (median=954 ng/g; max=12,189 ng/g; min=57 ng/g), but among the low-activity seep stations sampled here only aragonitic carbonates were recovered (median=436 ng/g, max=522 ng/g, min=377 ng/g). The three native-active-station carbonates which were aragonitic in composition exhibited the highest total IPL abundance (>4,180 ng/g; Fig. 1a). This high total IPL abundance was mirrored in the single rock transplanted from an active to low-activity station (11,757 ng/g), which happened to also be aragonitic. The remaining 19 of 23 samples all yielded IPL concentrations of less than 1,462 ng/g (mean=351 ng/g, σ =356 ng/g). Besides the three native carbonates with very high IPL abundances, the remaining 10 native carbonates were not differentiated in total IPL concentration by activity or mineralogy (mean_{active,calcitic/dolomitic}=445 ng/g; mean_{low-activity,aragonitic} =432 ng/g), although native-calcitic/dolomitic carbonates from active seep stations exhibited 10-fold wider variability (σ =588 ng/g) than native-aragonitic carbonates from low-activity seep stations (σ =59 ng/g). Transplanted carbonates yielded similar total IPL abundances to the native carbonates (Fig. 1a), while all four autoclaved colonization carbonates yielded very low amounts of IPLs (mean=76 ng/g, σ =37 ng/g). Pre-deployment negative controls of the colonization carbonates after autoclaving yielded no bacterial IPLs but detectable concentrations of uncharacterized archaeal IPLs (data not shown).

The four carbonates which hosted the highest total IPL concentrations (3 native and 1 transplant) also exhibited the four most depleted bulk organic carbon isotopic compositions (Table 1; Fig. 1c). The total dataset of 23 carbonates demonstrated a linear correlation between bulk $\delta^{13}\text{C}_{\text{org}}$ and total IPL concentration ($R^2=0.60$; $p \ll 0.01$) but no linear correlation between bulk organic $\delta^{13}\text{C}_{\text{org}}$ and total IPL concentration when the four carbonates with very high IPL

concentrations were excluded ($R^2=0.05$; $p=0.36$). Aragonitic carbonates, regardless of seep activity or experimental treatment, exhibited significantly more depleted bulk organic $\delta^{13}\text{C}$ (mean= $-49.0\pm 11.3\%$) than calcitic/dolomitic carbonates (mean= $-26.3\pm 3.3\%$).

Native carbonates with high total IPL concentrations exhibited high proportions of archaeal IPLs and low $\delta^{13}\text{C}_{\text{org}}$ values (Fig. 1d; Fig. S3; Table S2). A list of archaeal IPLs and their likely sources in cold seep systems is provided in the Supplementary Material (Table S3). These included phosphatidyl-inositol, phosphatidyl-glycerol, and phosphatidyl-serine hydroxyarchaeols (PI-, PG-, and PS-OH-AR), common among ANME-2 archaea, as well as monoglycosidic, diglycosidic, and phosphatidyl-glycerol glycerol-diphytanyl-glycerol-tetraethers (1G-, 2G-, and PG-GDGT) typically assigned to ANME-1 archaea (Fig. 1d; Table S3). Bacterial fractions of total IPLs were composed of a variety of non-isoprenoidal diacyl-glycerols (DAG), acyl-ether-glycerols (AEG), and diether-glycerols (DEG) with phospholipid head groups (Fig. 1d). The chemotaxonomy of these bacterial IPLs is not fully understood, although previous studies of seep core lipids have associated non-isoprenoidal glycerol ethers with sulfate-reducing *Deltaproteobacteria* (e.g. Hinrichs et al. 2000; Orphan et al. 2001; Elvert et al. 2003).

Archaeal IPLs were a more abundant fraction of the total IPLs on native-aragonitic carbonates as compared with native-calcitic/dolomitic carbonates (Fig. 2a), which was also reflected in the higher archaeal IPL proportion associated with carbonates from low-activity vs active stations (Fig. 2b). The median proportion of ANME-2-derived IPLs, identified as the sum of AR (including OH-AR) IPLs, among all IPLs, was also higher on aragonitic carbonates but with less of a clear differentiation by seep activity (Fig. 2). Among archaeal IPLs only, the median proportion of ANME-2-derived IPLs was only slightly higher in the native-aragonitic carbonates as compared to native-calcitic/dolomitic carbonates (Fig. 2a). Relative proportions of IPLs affiliated with ANME-2 among total archaeal IPLs were slightly higher in carbonates from active stations than low-activity stations (Fig. 2b). The median proportion of IPLs attributed to ANME-1 (all GDGTs divided by all archaeal IPLs) among all bacterial and archaeal IPLs was higher

among low-activity seep carbonates than active seep carbonates, but equivocal by mineralogy (Fig. 2). ANME-1 fractions among solely archaeal IPLs demonstrated similar, though less strong, distribution with regard to seep activity. Native-aragonitic rocks exhibited a higher and more variable fraction of PG-GDGTs among intact polar tetraethers than calcitic/dolomitic rocks, consistent with more contemporary/active ANME-1 biomass (Yoshinaga et al. 2015; Kellermann et al. 2016; Fig. 2a). Absolute abundances of the 2G-GDGT IPL on its own were higher in native-low-activity than native-active carbonates (Fig. 1; Fig. 7).

Over the whole ASL dataset, archaeal core lipids were more abundant than archaeal IPLs ($Avg_{core/IPL}=5$; $Max_{core/IPL}=16$, $Min_{core/IPL}=1$; Fig. 1e; Table S2). The core lipids were dominantly composed of GDGTs, while the IPLs were rich in AR and OH-AR (Fig. 1e; Table S2). ANME-2/Archaea_{Total} ratios were consistently lower by a factor of 3.2 ± 1.6 in the core lipids as compared to the IPLs recovered in the ASL dataset ($R^2=0.80$; Table S6). The ANME-2/Archaea_{Total} ratio was not consistent between IPLs in the ASL and IPL datasets, which may be derived from methodological differences in the data acquisition or represent differences in fossil vs extant archaea.

Whether analyzing the IPL or ASL datasets, aragonites were observed to host the highest richness of lipid biomarkers (Fig. S1). However, in all three of the IPL, ASL, and 16S rRNA gene datasets the plurality of lipids were cosmopolitan to all mineralogy types (Fig. S1; raw data used to generate each Venn diagram in Fig. S1 is given in Table S5). Decomposing the IPL and ASL datasets from the native-active carbonates by mineralogy again revealed the archaeal IPLs to be more associated with aragonitic than calcitic/dolomitic carbonates (Fig. 3), with bacterial IPLs (IPL dataset) and core archaeal lipids (ASL dataset) more associated with calcitic/dolomitic than aragonitic carbonates. Some abundant non-isoprenoidal ester- and ether- bound bacterial IPLs (e.g., PC-DAG-C33:1, PC-DAG-C31:0, PG-DEG-C36:2), tentatively assigned to sulfate reducing bacteria, appeared to be more strongly associated with dolomitic than calcitic mineralogy (Fig. 3a).

Non-metric multidimensional scaling (NMDS) ordinations of IPL profiles from the native and transplantation carbonates revealed some differences as compared to corresponding 16S rRNA gene diversity surveys (Fig. 4). Unlike 16S rRNA gene trends, the native samples are not statistically differentiated by seep activity among the IPL dataset. This difference is driven by the native-active samples clustering into two distinct groups (separated by mineralogy) while the native-low-activity carbonates cluster into one distinct group (all of which exhibit aragonitic mineralogy). Mineralogy was also observed to differentiate the 16S rRNA gene profiles, although in that dataset seep activity was more strongly associated with inter-sample DNA-based differences. IPL profiles from replicate transplanted carbonates at duplicate seafloor stations did not generally demonstrate a shift in microbial community over the 13 month experiment. IPL diversity profiles from neither native nor transplant carbonates were differentiated by $\delta^{13}\text{C}_{\text{org}}$ or seafloor sampling station (Fig. S2).

When examining IPL richness, we find a large proportion of lipids to be cosmopolitan to all samples – present in the transplants and both activity classes of native carbonates (n=47 in Fig. 5a; n=91 in Fig. 5b). However, clear loss of active-type biomarkers and gain of low-activity-type biomarkers is apparent from transplant experiments upon 13 months of seep quiescence. Twenty-eight percent (station HR-3/-4 in Fig. 5a) and 30% (station HR-7/-8 in Fig. 5b) of the IPLs present in native-active carbonates were lost after 13 months of seep dormancy in transplanted carbonates. Meanwhile, the appearance of IPLs characteristic of background carbonates (e.g., from low-activity sites) is slower – after 13 months, only 11% (station HR-3/-4 in Fig. 5a) and 4% (station HR-7/-8 in Fig. 5b) of the IPLs present in native-low-activity carbonates have appeared in the transplant carbonates.

Modeling reveals highly similar time-dependent richness evolution for both the 16S rRNA gene and IPL biomarkers, at both experimental stations (Fig. 6). However, 16S rRNA gene biomarkers incur a more dramatic decrease in richness, down to ~40% of maximum richness, whereas IPL biomarkers do not decrease beyond ~70% of maximum richness (Fig. 6b-c). This

may be due to partly to genuinely higher magnitude of loss and gain within the 16S rRNA gene biomarker pool and partly to the level of taxonomic depth afforded by gene sequencing vs IPL analysis. Notably, the archaeal core lipids do not exhibit this behavior, instead only accumulating biomarker richness over time, consistent with higher recalcitrance to degradation. After ~100 years of modeled time, very little remaining biomarker richness change is predicted.

Identification of specific IPL and 16S rRNA gene biomarkers characteristic of active or low activity conditions revealed 6 diagnostic IPLs and 11 diagnostic 16S rRNA gene OTUs in the dataset (out of 201 IPLs and 1,057 16S rRNA gene OTUs total) that may represent robust biomarkers characteristic of seep activity (Fig. 7; Fig. 8; Table 3). Of the IPL biomarkers, which included 5 bacterial (all diacylglycerol [DAG] IPLs) and 1 archaeal IPL (2G-GDGT), the 5 bacterial IPLs were diagnostic of active seepage conditions and the 1 archaeal IPL was diagnostic of low-activity conditions. Of the 16S rRNA gene biomarkers, which also included bacterial and archaeal OTUs (e.g., *Desulfobulbaceae*, and ANME-1b), 5 were characteristic of active seepage conditions and 6 were characteristic of low-activity conditions. All ten of the combined IPL and 16S rRNA gene biomarkers diagnostic of active seep conditions responded relatively rapidly to seep quiescence, with modeling revealing them to be >90% transitioned (i.e., decreased in abundance to low-activity seep levels) within 10 years (Fig. 8a,e). Biomarkers diagnostic of low-activity seepage responded more slowly, with only 2 of the 7 biomarkers (the ANME-1b and *Brocadiaaceae* 16S rRNA gene OTUs) being >90% transitioned (i.e., increased in abundance to low-activity levels) within 10 years of modeled time (Fig. 8f).

3.4 DISCUSSION

3.4.1 COMPARISON OF 16S rRNA GENE, IPL, AND CORE LIPID BIOMARKERS

The taphonomic process by which microbial biomarkers are recoded in seep carbonates is not well understood, and the extent of preservation may vary for 16S rRNA genes vs intact

polar lipids vs core lipids. Accurate interpretation of ancient seep carbonates for the purpose of reconstructing paleo-microbiota and carbon cycles is dependent on whether and to what extent seep carbonates record microbial bio-signatures reflective of the assemblages during active seepage. This study presents several lines of evidence suggesting that IPL biomarker profiles in native seep carbonates integrate a period of time only slightly longer than 16S rRNA genes, and that neither represent an integration time as long as core lipids.

Three primary observations from the 16S rRNA gene data described in Case et al. (2015) indicated that gene biomarkers principally recorded the extant microbial community and that carbonate-associated microbial communities underwent succession upon seep quiescence in our 13-month *in situ* transplantation experiments: (i) a difference in 16S rRNA gene community structure (beta diversity) was observed in microbial assemblages inhabiting native active vs low-activity carbonates, (ii) 16S rRNA gene richness (alpha diversity) decreased upon seep quiescence, and (iii) specific activity-sensitive OTUs (e.g., *Helicobacteraceae*) clearly responded to imposed changes in seep activity (Fig. 1,2,5 in Case et al. 2015). In order to examine whether IPLs, like DNA-based diversity surveys, also reflect the extant microbial community's shifts on short (13-month) timescales, we analyzed IPLs from the same carbonate sample set as described in Case et al. (2015) to look for similar patterns of biomarker behavior. In addition, the quantitative nature of the IPL dataset allowed us to probe shifts in absolute abundance and estimate total cell concentrations – interpretations not possible in PCR-based 16S rRNA gene surveys which rely on relative abundance.

Unlike in the 16S rRNA gene data, ordination of the IPL data did not reveal seepage activity to statistically differentiate the native-active and native-low-activity assemblages ($p=0.07$ for relative abundance IPL data; $p=0.13$ for absolute abundance IPL data; Fig. 4b-c). This either suggests that IPLs record a more homogenized (time-integrated) biomarker inventory than 16S rRNA genes or that IPL biomarkers are recorded in carbonates exclusively during periods of active seepage and subsequently change very little upon seep quiescence. However, we note that

the ordination does not reveal a highly homogenized mixture of native samples, but rather three distinct clusters: one of native-low-activity carbonates (all aragonitic) and two of native-active carbonates, which are separated by mineralogy (Fig. 4b-c). Interestingly, the two mineralogy-separated clusters of native-active carbonates are differentiated by, among others, the absolute abundances of PC-DAG-C34:2 (calcite/dolomite) and PS-OH-AR (aragonite; a putative ANME-2 biomarker). Overall, while mineralogy is strongly associated with differences in microbial assemblages (as was also the case for 16S rRNA genes), the effect of seep activity also seems to play a role. The clustering of native-low-activity carbonates separate from both native-active clusters implies storage of distinct IPL biomarker inventories as a function of seep activity, which would be the case if IPL inventories eventually shift between active and low activity seepage periods. Moreover, the aragonitic carbonates are well-differentiated into active and low-activity groups. This is supported by analysis of specific IPL ratios, which indicate the proportion of archaea to total microorganisms as well as the proportion of ANME-1 among total IPLs is different in active vs low-activity environments (ANME-1, specifically, higher in low-activity settings; Fig. 2b).

Complex cycling of biomarkers (simultaneous loss of active-type and gain of low-activity-type biomarkers), rather than passive biomarker accumulation over time, would be supported by a decrease in richness upon imposed seep quiescence (our transplant-to-low-activity experiments) as the microbial assemblage responds to changing conditions. Indeed this was observed in the 16S rRNA gene data, and it is also observed in the IPL data (Fig. 5; Raw data used to generate Fig. 5 is given in Table S5). While both biomarkers indicate a decrease in richness upon seep quiescence, we note that the majority of IPL richness is cosmopolitan to all samples (Fig. 5), while the majority of 16S rRNA gene richness was specific to either active or low-activity seepage conditions (Fig. 3b-c in Case et al. 2015). This fundamental difference complements the NMDS ordinations, implying that IPL biomarkers overall have distributions similar to 16S rRNA genes but with more tendency to exhibit cosmopolitan, shared, and/or time-integrated aspects.

If microbial assemblages respond to seep quiescence, and the response is reflected in biomarker patterns on short timescales, then specific biomarkers ought to be identifiable which exhibit a rise (or fall) in abundance during the transition. This was clear in 16S rRNA gene data, where OTUs associated with the *Helicobacteraceae* and *Methylococcales* (putative sulfur and methane oxidizers, respectively), as well as ANME-1b (anaerobic methanotrophs) clearly shifted in relative abundance during the transplantation experiments (Fig. 4 in Case et al. 2015). Not only are IPL biomarkers also identifiable which demonstrate short timescale response to changes in seep activity, but some IPL biomarkers have similar putative chemotaxonomy as the 16S rRNA OTUs (Fig. 7). For example, IPLs and OTUs associated with ANME-1 both increased in relative abundance. This similar biomarker recovery suggests IPLs are recording contemporary changes in the microbial community, at least for some microorganisms. Furthermore, the quantitative nature of the IPL dataset enables examination of similar (or different) lipid biomarker shifts in absolute vs relative abundance. Among the ANME-1 IPLs, for example, an increase upon transition to low-activity conditions was observed in both absolute and relative abundance, but the magnitude of shift was lesser in absolute than relative units. Among bacterial IPLs, we observed that those which decrease in absolute abundance upon seep quiescence (e.g., PC-DAG-C34:2) also decrease in relative abundance (Fig. 7; Fig. 8).

It therefore appears that IPL biomarkers are distributed in a broadly similar manner as 16S rRNA genes and exhibit roughly similar shifts in pattern upon imposed changes in seep activity. As such, IPLs may reflect extant microbial communities as previously suggested (White et al. 1979; 1997; Zink et al. 2003; Sturt et al. 2004). However, other lines of evidence imply a degree of recalcitrance within the IPL biomarker pool that would require IPLs to reflect a somewhat longer time-integration than the 16S rRNA genes.

Firstly, IPLs appear recalcitrant to degradation as evidenced by the recovery of high IPL concentration in the aragonitic carbonate transplanted from an active to low-activity seep station (Fig. 1a). Secondly, in NMDS ordination the transplant-to-active carbonates plot near the native

carbonates from the low-activity regimes in which they originated (Fig. 4b). This was not the case in 16S rRNA gene data, where transplants simulating seep activation revealed a rapid response of the microbial assemblages to renewed methane flux (Fig. 1b in Case et al. 2015). Thirdly, as already pointed out above, the majority of IPL richness is cosmopolitan to all carbonates (Fig. 5), implying longer-term storage of biomarker inventories than 16S rRNA gene OTUs where the majority of richness was specific to either active or low-activity conditions (Fig. 3b-c in Case et al. 2015). Finally, the proportion of GDGTs with phosphatidyl-glycerol head groups (PG-GDGT), which are suggested to be a proxy for active ANME-1 cells (Kellermann et al. 2016), are a minority of all GDGT IPLs (Fig. 2). This points to a large proportion of GDGT IPLs being either historic or perhaps produced in stationary phase rather than by actively growing cells (Kellermann et al. 2016).

It appears that IPLs represent a biomarker inventory with somewhat greater longevity than 16S rRNA genes, but how do IPLs compare to core lipids, which are hypothesized to be the best biomarker recording ancient seep microorganisms and processes (e.g., Birgel et al. 2008b)? The independent archaeal lipid dataset (ASL) is well-suited to this inquiry – archaeal intact polar and core lipids can be directly contrasted. The ASL dataset reveals seep carbonates to host a higher amount of archaeal core lipids than IPLs by a factor of up to 16 (Fig. 1e), supporting a fossil record of historic microorganisms (the core lipids) stored in seep carbonates. However, the specific profiles of archaeal lipids differ whether viewed as IPLs or core lipids, specifically the ANME-2/Archaea_{Total} ratio which tends to be lower in core lipids than IPLs (Table S6). This ratio is of interest in geobiological studies due to the interpretation that ANME-1 and ANME-2 are physiologically adapted to low and high flux methane supplies, respectively (Niemann and Elvert 2008; Birgel et al. 2011; Natalicchio et al. 2015). The marked difference in ANME-2/Archaea_{Total} ratios between archaeal intact polar and core lipid data is evidence that the core lipids likely preserve a biomarker inventory with even longer integration time than IPLs. The core

lipid record is likely impacted by the specific longevity of GDGTs as hypothesized by Kellermann et al. (2016).

3.4.2 MODELED TIME-DEPENDENT BIOMARKER PROFILE CHANGES

3.4.2.1 SHIFTS IN COMMUNITY RICHNESS UPON SEEP QUIESCENCE

Our parallel biomarker datasets indicate increasing longevity of biomarkers from 16S rRNA genes to IPLs to core lipids. By extrapolating our transplant experiment results beyond 13 months, we can further inform the timescales of biomarker profile changes upon seep quiescence – both the richness of the entire microbial assemblage as well as the concentrations of specific “active-type” or “low-activity-type” biomarkers.

From the richness models, it is possible to define three phases of microbial community change upon seep quiescence: (i) a phase of rapid richness loss (approximately the first and second years), (ii) a phase of relatively rapid richness gain (approximately through the first decade), and (iii) a relatively slow transition to the new stable state of the microbial assemblage (approximately year 10 onward). 16S rRNA gene biomarkers demonstrate a larger relative decrease in richness – Phase (i) – than IPL biomarkers (Fig. 6b,c). Both biomarkers are reduced in richness to approximately the level of the core “cosmopolitan” richness (dashed horizontal lines in Fig. 6) before rebounding to higher richness levels. This core richness could be interpreted as either evidence for a pool of stored fossil biomarkers, or as evidence of a core microbial community whose constituent members have no sensitivity to seep flux, and therefore whose presence does not change upon seep quiescence.

A fundamental difference between the IPL and 16S rRNA gene datasets is that the majority of richness in IPLs is cosmopolitan to all samples, but for 16S rRNA genes the majority of richness is specific to either active or low-activity conditions. Therefore, the process of biomarker profile change is inherently different: IPLs are undergoing a subtle shift in the

presence/absence of a minority of the overall IPL profile, while 16S rRNA gene biomarkers are turning over the majority of the presence/absence community profile between two significantly different microbial assemblage types (active and low-activity). The longevity of IPLs in subsurface settings is not well constrained, with some estimates that IPLs represent living biomass and some that IPLs, especially archaeal IPLs, may degrade extremely slowly (Logemann et al. 2011; Xie et al. 2013). Our data over 13-month experiments are consistent with IPLs exhibiting longevity more similar to DNA than core lipids, and therefore that on these approximately year-long timescales IPLs tend to reflect extant microbial assemblages. This incongruity with recent evidence of long-lived IPLs is perhaps rooted in different methodological approaches: our experiments were performed *in situ*, with analysis of biomarkers from genuine seep microorganisms, while recent studies either employed synthetic analogs of a single archaeal IPL type (Xie et al. 2013) or amended laboratory incubations with cells not representative of methane seep microbial diversity (Logemann et al. 2011). Although even DNA has been questioned as reflective of extant microorganisms (Dell'Anno et al. 1998; Levy-Booth et al. 2007; Torti et al. 2015), evidence of microbial assemblage shifts in our 16S rRNA dataset strongly suggests a reflection of contemporary microbial community dynamics.

3.4.2.2 CHANGES OF BIOMARKERS CHARACTERISTIC TO ACTIVE OR LOW-ACTIVITY SEEP REGIMES

It appears from 16S rRNA gene data (Case et al. 2015) and modeling (this study) that microbial assemblages do change upon seep quiescence, and that several decades are necessary for community structure to fully respond to changing conditions. Concurrent with these changes, carbonates at low-activity seep sites nonetheless still host viable anaerobic methanotrophs (Marlow et al. 2016a). IPL profiles appear to preserve a slightly more historic whole-assemblage record than 16S rRNA genes, with a smaller proportion of the IPL profile than the 16S rRNA

gene profile shifting upon seep quiescence (Fig. 6). However, concentrations of a subset of individual IPL (and 16S rRNA gene) biomarkers do appear to be sensitive to seep activity (Fig. 7). These included bacterial and archaeal IPLs (e.g., PC-DAG-C34:2 and 2G-GDGT) as well as bacterial and archaeal 16S rRNA gene OTUs (e.g., Desulfobacteraceae and ANME-1b). Cross-correlation of the lipid and 16S rRNA gene datasets supports that some of these characteristic biomarkers may in fact represent the same microbial clades. The PE-DAG-C30:1 IPL, though not strongly correlated with any of the diagnostic 16S rRNA gene OTUs, is strongly associated with another *Helicobacteraceae* OTU in the 16S rRNA gene dataset (Table S4), a sulfur-oxidizing epsilonproteobacterial family known to be sensitive to seep activity (Case et al. 2015). All detected lipid-DNA correlations are provided in full in Table S4, although we note that apparent correlations may arise not because an IPL is specifically produced by a microbial species, but because distributions of some microbial species are correlated with each other (e.g., Trembath-Reichert et al. 2016) and therefore their constituent IPLs may be correlated as well. In addition, it is difficult to identify specific chemotaxonomic connections between IPLs and specific microbial taxa without pure cultures of diverse environmental microorganisms with which to probe species-specific IPL production.

Modeling for the 11 16S rRNA gene biomarkers predicted that 7 of 11, including all 5 active-type biomarkers, would be >90% transitioned to values observed in the low-activity sites within 10 years (Fig. 8). Thus, the response of key activity-sensitive IPL and 16S rRNA gene biomarkers to seep quiescence is, as expected, shorter than the whole-community response (Fig. 6, Fig. 8). It is possible this approach could, in future studies, be applied to differentiate endogenous vs exogenous inputs to microbial biomarker inventories in other marine environments, for example where pelagic and sedimentary signals are mixed (Blumenberg et al. 2015; Pearson et al. 2016).

Of the five characteristic active-type bacterial IPLs (Fig. 7), PC-DAG-C43:2 was recovered in especially high relative abundance on the colonization carbonates (mean=8%,

min=2%, max=17%, Table S2), notable because bacterial IPLs were not recoverable from pre-incubation sterilized negative controls of the colonization experiments. However, patterns of colonization by microorganisms producing PC-DAG-C34:2 did not seem to be activity-dependent, as both the maximum and minimum relative abundance values were recovered from the two carbonates placed for colonization at low-activity seep stations (the same was true for absolute abundance values; Table S2).

Notably, in both IPL and 16S rRNA gene analyses, putative biomarkers for ANME-1 archaea (2G-GDGT among the IPLs, ANME-1 OTUs among the 16S rRNA genes) are predicted to increase in abundance during the shift to a low-activity seepage environment (Fig. 7). This is in concordance with previous studies in which ANME-1 biomarkers were assumed to represent a low-flux seepage regime (Blumenberg et al. 2004; Peckmann et al. 2009) and in which ANME-1 OTUs were observed to both natively inhabit and actively colonize low-activity seep carbonates at a higher relative abundance than at active seeps (Marlow et al. 2014b; Case et al. 2015). We can determine from our quantitative IPL data that the increase in 2G-GDGT relative abundance is at least partly a function of decreasing total IPL content rather than in-growth of new organisms in low-activity conditions, similar to 16S rRNA gene data from Marlow et al. (2014a). Median absolute abundance of the 2G-GDGT IPL is 14 times higher in the native-low-activity (median=33.0 ng/g; Q1=27.7 ng/g; Q3=55.5 ng/g) than in the native-active (median=2.4 ng/g; Q1=0.5 ng/g; Q3=21.9 ng/g) carbonates. However, median relative abundances of 2G-GDGT are 20 times higher in native-low-activity (median=7.6%; Q1=7.3%, Q3=10.6%) than native-active (median=0.4%; Q1=0.4%; Q3=0.5%) carbonates. Therefore of the increase in relative abundance of the 2G-GDGT IPL upon seep quiescence, approximately 70% of the signal is supported by a genuine increase in absolute abundance and approximately 30% of the signal is due to the degradation of other IPLs in the dataset. This is also reflected in estimates of cell concentrations (see below). ANME-1b OTUs were observed to actively colonize sterilized seep carbonates on short timescales in 16S rRNA gene data (Case et al. 2015), but

similar interpretation is difficult with the IPL dataset due to the recovery of archaeal IPLs in the pre-colonization negative controls. The observations in the IPL dataset are supported by the independent archaea-specific ASL dataset, in which 2G-GDGT IPLs are also observed to increase in relative abundance in the native-low-activity carbonates (Fig. 1), but absolute abundances are not available for the ASL dataset. Furthermore, an independent stable isotope labeling study of sediment-hosted seep microbial communities concluded that 2G-GDGT IPLs were likely produced by ANME-1 cells in stationary phase rather than actively growing (Kellermann et al. 2016). Over time the core lipids appear biased toward ANME-1 GDGT lipids over ANME-2 AR and OH-AR lipids, probably as a result of slow degradation rates of GDGTs. Thus caution must be used when interpreting ancient seep biomarker profiles as fully representative of historic seep conditions and processes, an application which has already begun to be explored (Birgel et al. 2006a; Niemann and Elvert 2008; Peckmann et al. 2009; Birgel et al. 2011; Natalicchio et al. 2015).

3.4.3 ESTIMATES OF MICROBIAL CELL CONCENTRATION ASSOCIATED WITH SEEP CARBONATES

Previous evidence, though limited in scope, suggests that carbonates from active seepage regimes exhibit higher porosity, permeability, rates of methane oxidation, total microbial cell concentration, and ANME-2 relative abundance than carbonates from low activity settings (Marlow et al. 2014a; b). In order to convert from ng/g to cell/cm³, we applied multiple theoretical and empirical conversion factors for the density of seep carbonates and the cellular mass of IPLs (Supplemental Text; Simon and Azam 1989; Zink et al. 2008; Lipp et al. 2008; Meador et al. 2014; Marlow et al. 2014a) (Fig. 9). These estimates corroborate the finding by Marlow et al. (2014a) that active carbonates can host microbial abundances on the order of 10⁹-10¹⁰ cell/cm³. Our data also suggest that some seep carbonates may host cell concentrations

several orders of magnitude lower than estimated by DAPI cell counts in Marlow et al. (2014a) (Fig. 1b; Supp. Text S3). Differences could be explained by natural heterogeneity, under-efficiency of lipid extraction (which can not be ruled out), or overestimation of cell concentration in Marlow et al. (2014a), for example by extrapolating the number of cells from raw counts of microbial aggregates. With our quantified IPL dataset we were able to estimate median ANME-1 absolute cell concentrations, calculated as the sum of GDGTs (Table S3), of 1.1×10^7 cell/cm³ (Q1= 1.0×10^7 ; Q3= 1.1×10^8) in native-active carbonates and 9.1×10^7 cell/cm³ (Q1= 8.3×10^7 ; Q3= 1.7×10^8) in native-low-activity carbonates (Fig. 9a). Likewise ANME-2 IPLs (calculated as the sum of all AR and OH-AR) gave median absolute cell concentrations of 3.9×10^7 cell/cm³ (Q1= 1.2×10^7 ; Q3= 4.2×10^9) in native-active carbonates and 1.9×10^8 cell/cm³ (Q1= 1.8×10^8 ; Q3= 1.9×10^8) in native-low-activity carbonates (Fig. 9a). Although it is surprising that the ANME-2 IPLs reveal a higher cell concentration of ANME-2 in low-activity than active seep stations, we note that the variability of ANME-2 IPLs is very wide among native-active carbonates. In fact, the description of the data is improved by binning not only according to seep activity but additionally by mineralogy. This reveals three groupings: active-calcitic/dolomitic, active-aragonitic, and low-activity-aragonitic (unfortunately, low-activity-calcitic/dolomitic carbonates were not present in the sample set). When plotting the data within these groupings, it is clear that the carbonates from active stations are separated into two groups: aragonitic, with very high cell concentrations, and calcitic/dolomitic with lower cell concentrations (Fig. 9b). This was apparent, of course, in the total cell concentrations (Fig. 1a) and in the NMDS ordinations of the data (Fig. 4b-c). Within solely aragonitic rocks (thus removing the affect of mineralogy), ANME-2 cell counts are shown to decrease from active to low-activity stations, as expected (Fig. 9b). Within only aragonitic rocks the ANME-1 cell counts are observed to be highly similar between active and low-activity conditions, and when including the calcitic/dolomitic carbonates it further appears that over the whole data set, the ANME-1 increase in abundance from active to low-activity conditions.

In order to make a comparison to active-type Hydrate Ridge seep sediments, we averaged aggregate counts (aggregates/cm³) from the top 3 centimeters below seafloor of *Beggiatoa* fields at Hydrate Ridge reported in Boetius et al. 2000 and Treude et al. 2003, and converted to total cells/cm³ using conversion factors reported for active-type sediments in Marlow et al. (2014a). We then calculated the proportion of total cells in near-surface Hydrate Ridge active-type sediments attributable to ANME-1 and ANME-2 using proportions reported in Knittel et al. 2005, assuming reported aggregates were 50:50 ANME-2:bacteria and single cells were 100% ANME-1. Propagating uncertainty, we find ANME-1 and ANME-2 to be present at 5.9x10⁷-to-1.5x10⁸ and 2.6x10⁹-to-6.6x10⁹ cell/cm³, respectively (Fig. 9). These numbers are remarkably comparable to our calculations of ANME-1 and ANME-2 cell concentrations estimated from IPLs recovered in Hydrate Ridge active seep carbonates, suggesting carbonates host similar magnitudes of biomass as seep sediments.

3.4.4 ASSOCIATIONS BETWEEN BIOMARKERS AND MINERALOGY

Beyond the induction of authigenic carbonate formation by alkalinity generation during sulfate-coupled AOM (Berner 1980), the mechanistic links between mineralogy, microbial assemblage, and precipitation processes remain unclear (Teichert et al. 2005; Reitner et al. 2005; Leefmann et al. 2008; Birgel et al. 2011; Hagemann et al. 2012). Carbonates are hypothesized to form within the sediment column, with aragonites likely to form nearest the sediment/water interface where high sulfate concentrations inhibit precipitation of Mg-bearing minerals such as dolomite and high-Mg calcite (Burton 1993; Greinert et al. 2001; Aloisi et al. 2002). That our dataset shows some IPLs to be preferentially associated with dolomite is intriguing (Fig. 3a), as sulfate-reducing bacteria (SRB) are known to be involved in the precipitation of dolomite (Vasconcelos et al. 1995; Van Lith et al. 2003; Warthmann et al. 2005). Sulfate-reducing delta-proteobacteria *Desulfosarcina variabilis* and *Desulforhabdus amnigenus* produce non-isoprenoidal

ether- and ester-bound lipids (AEG, DEG, DAG) with a variety of polar head groups (PC, PE, PG; Rütters et al. 2001). Core and intact polar versions of these lipids have also been recovered in environmental samples heavily enriched in the *Desulfosarcina*, *Desulfococcus*, and *Desulfobulbus* genera which are known syntrophic partners of anaerobic methanotrophs (Hinrichs et al. 2000; Orphan et al. 2001; Pancost et al. 2001; Elvert et al. 2003; Rossel et al. 2008; Niemann and Elvert 2008; Schubotz et al. 2011). Association of similar lipids in this study with dolomitic carbonates renews questions regarding the timing and location of dolomite precipitation in seep sediments. Alkalinity generation by AOM consortia could help promote dolomite precipitation, but dolomites are often observed to have relatively enriched $\delta^{13}\text{C}$ values relative to methanotrophy (e.g. Kulm and Suess 1990; Greinert et al. 2001). A separate SRB community could be involved in the precipitation of dolomite, but presumably would need to be near the sediment/water interface where sulfate concentrations remain high (Schubotz et al. 2011). Previous models, in contrast, have suggested dolomites form deep in the sediment column, below the sulfate-methane transition zone (e.g. Greinert et al. 2001). Thus, the interrelationship between SRB, AOM, sulfate, and dolomite remains enigmatic.

3.5 CONCLUSIONS: OPPORTUNITIES AND CHALLENGES FOR RECONSTRUCTION OF PAST METHANE SEEPS

Interpretation of biological and chemical signatures recorded in carbonates from ancient methane seeps has great potential to inform our understanding of historic microbial community structure and carbon cycling on Earth. However, the taphonomy of microbial biomarkers has not been experimentally tested. Lipid biomarker evidence presented here from Hydrate Ridge, OR, suggests that IPL biomarkers demonstrate behavior more similar to 16S rRNA genes than complementary core lipids. Relative abundances of some individual IPLs (e.g., PC-DAG-C34:2, 2G-GDGT) are especially sensitive to changing seep flux and therefore informative as to whether

an “active-type” or “low-activity-type” microbial assemblage is recorded in seep carbonates. In the future, transplant experiments with more time points and better resolved geochemical data can further shed light on shifts in microbial community structure during response to environmental change.

IPL distributions were correlated partly with carbonate mineralogy. Aragonitic carbonates hosted IPLs most representative of active seep conditions, including depleted $\delta^{13}\text{C}_{\text{org}}$ values and high ANME-2 abundances (i.e., ARs and OH-ARs). In contrast some bacterial IPLs, including those with ester- and ether-linkages, were preferentially recovered on dolomitic carbonates (e.g., PC-DAG-C33:1, PC-DAG-C31:0, PG-DEG-C36:2). Although chemotaxonomy of these lipids is challenging, the preponderance of evidence suggests they are likely associated with sulfate-reducing bacteria.

Our quantitative IPL dataset confirms the carbonate-hosted cell concentrations determined previously by DAPI staining (Marlow et al. 2014b), but suggests greater variability among carbonates than previously observed. The concentrations of ANME-1 and ANME-2 are similar to estimates from active Hydrate Ridge seep sediments, further corroborating that seep carbonates likely play critical roles in carbon cycling both today and, potentially, in Earth’s past. Accurately interpreting biomarker records of paleo-seepage, however, remains challenging due to variable rates of methane flux, microbial response, and biomarker degradation.

3.6 ACKNOWLEDGMENTS

We thank Lisa Levin for helping orchestrate the experimental design and field work. In addition, we thank the crews of *R/V Atlantis* cruises 15-68 and 18-10 for their help at sea, without which this work would not have been possible. Members of the VO research group, including Stephanie Connon, Joshua Steele, Fuyan Li, and Jeffrey Marlow helped with at-sea processing and laboratory work. DC was supported by a National Science Foundation (NSF) Graduate

Research Fellowship. Research funding for VO was provided by the NSF (OCE-0825791), the NASA Astrobiology Institute (NNA13AA92A), and the Gordon and Betty Moore Foundation Marine Microbiology Initiative #3780. This is NAI-Life Underground Publication Number 077. Funding for AP was provided through an NSF-Division of Ocean Sciences Postdoctoral Research Fellowship.

3.7 TABLES

Table 1. All samples in this study are listed with their accompanying metadata. Samples are organized by the three different experimental treatments in the study: native samples (exhumed *in situ* carbonates), transplantation samples (seafloor manipulation experiments), and colonization samples (deployed sterile carbonate substrates).

Experimental Treatment	Activity	Sample Number	Specific Hydrate Ridge Geography	Seafloor Station	Latitude (Decimal °N)	Longitude (Decimal °W)	Depth (mbsl)	Carbonate Mineralogy ^a	Percent Aragonite (±15%)	Percent Calcite (±15%)	Percent Dolomite (±15%)	Total IPL Recovery (ng/g)	Cell Concentration (cells/cm ³) ^b	Bulk $\delta^{13}C_{org}$ (‰)
Native	Active	3530	North	HR-3	44.669544	125.098057	587	Aragonitic	70	23	7	11031	1.31E+09	-65.5
		5330	South	HR-V1	44.570239	125.147023	775	Aragonitic	80	18	2	4180	5.44E+08	-54.9
		5122	North	HR-7	44.667079	125.100033	601	Aragonitic	68	28	4	12189	1.59E+09	-61.5
		5109	North	HR-3	44.669463	125.098120	587	Calcitic/Dolomitic	40	38	22	144	1.88E+07	-25.1
		5110	North	HR-3	44.669481	125.098095	587	Calcitic/Dolomitic	14	57	29	117	1.52E+07	-24.0
		5112	North	HR-3	44.669481	125.098107	587	Calcitic/Dolomitic	44	38	18	57	7.42E+06	-23.9
	Low Act.	5123	North	HR-7	44.667079	125.100033	601	Calcitic/Dolomitic	24	26	50	446	5.81E+07	-28.1
		5120	North	HR-7	44.667079	125.100020	601	Calcitic/Dolomitic	44	0	56	1462	1.90E+08	-26.2
		5038	North	HR-4	44.670075	125.098674	595	Aragonitic	86	4	10	436	5.68E+07	-53.4
		3511	North	HR-5	44.669382	125.103619	620	Aragonitic	81	18	0	443	5.77E+07	-30.6
		5040	North	HR-4	44.670075	125.098674	595	Aragonitic	76	23	0	383	4.98E+07	-49.0
		5189	North	HR-8	44.667645	125.100712	604	Aragonitic	70	21	9	522	6.80E+07	-35.7
Transplantation	Low Act. -> Act.	5190	North	HR-8	44.667645	125.100712	604	Aragonitic	62	36	2	377	4.91E+07	-42.9
		5111	North	HR-3	44.669463	125.098120	587	Aragonitic	85	4	12	220	2.86E+07	-43.6
		5121	North	HR-7	44.667079	125.100020	601	Aragonitic	66	29	4	959	1.25E+08	-40.7
		5193	North	HR-8	44.667627	125.100712	603	Aragonitic	71	22	6	11757	1.53E+09	-60.9
	Act. -> Low Act.	5039	North	HR-4	44.670093	125.098699	595	Calcitic/Dolomitic	48	32	20	115	1.50E+07	-22.7
		5093	North	HR-4	44.670084	125.098686	595	Calcitic/Dolomitic	18	57	25	504	6.56E+07	-28.1
		5194	North	HR-8	44.667627	125.100712	603	Calcitic/Dolomitic	0	19	81	171	2.23E+07	-24.1
		5025c	North	HR-3	44.669454	125.098145	588	Calcitic/Dolomitic	34	51	15	112	1.59E+07	-34.1
Colonization	Active	5025d	North	HR-3	44.669454	125.098145	588	Calcitic/Dolomitic	0	4	96	90	1.17E+07	-24.3
		5145c	North	HR-4	44.670075	125.098661	600	Calcitic/Dolomitic	41	49	10	76	9.84E+06	-30.3
	Low Act.	5145d	North	HR-4	44.670075	125.098661	600	Calcitic/Dolomitic	13	0	86	25	3.24E+06	-24.1

^aSee Supplemental Text for details regarding mineralogical assignments; carbonates less >50% aragonite were binned "aragonitic" and those with <50% aragonite were binned "calcitic/dolomitic".

^bSee Supplemental Text for details regarding conversion of IPL concentration to volumetric cell abundance.

Table 2. Values of terms *a*, *b*, and *c* in the model of biomarker richness as a function of time (Equation 1). Values for IPL biomarkers are from Fig. 5 in this study. Values for 16S rRNA gene biomarkers are from Fig. 4 in Case et al., 2015. Term *a* is the cosmopolitan richness never lost nor gained (*a* constant). Term *b* is the remaining amount of active-type richness, a vector decreasing with time. Term *c* is the gained low-activity-type richness, an increasing vector with time. Time point *t*=0 is the richness of the native-active carbonates. Time point *t*=1.08 is the richness of the transplant-to-low-activity carbonates. The “infinite” time point is the eventual value to be achieved in the native-low-activity carbonates. See Supplemental Text for additional details.

16S rRNA Biomarkers						
Time (Years)	HR-3/-4			HR-7/-8		
	Term <i>a</i>	Term <i>b</i>	Term <i>c</i>	Term <i>a</i>	Term <i>b</i>	Term <i>c</i>
<i>t</i> =0	75	269	0	95	224	0
<i>t</i> =1.08	75	36	28	95	57	37
<i>t</i> =inf.	75	0	387	95	0	343
	$a(t) = 47$	$b(t) = \exp(-1.8565t+5.5947)$	$c(t) = 387 - \exp(-0.0693t+5.9584)$	$a(t) = 95$	$b(t) = \exp(-1.2633t+5.4116)$	$c(t) = 343 - \exp(-0.1054t+5.8377)$

IPL Dataset (IPLs of Archaea and Bacteria)						
Time (Years)	HR-3/-4			HR-7/-8		
	Term <i>a</i>	Term <i>b</i>	Term <i>c</i>	Term <i>a</i>	Term <i>b</i>	Term <i>c</i>
<i>t</i> =0	47	38	0	91	58	0
<i>t</i> =1.08	47	14	10	91	13	5
<i>t</i> =inf.	47	0	48	91	0	45
	$a(t) = 47$	$b(t) = \exp(-0.9217t+3.6376)$	$c(t) = 48 - \exp(-0.2156t+3.8712)$	$a(t) = 91$	$b(t) = \exp(-1.3805t+4.0604)$	$c(t) = 45 - \exp(-0.1087t+3.8067)$

ASL Dataset (intact polar and core lipids of Archaea only)						
Time (Years)	HR-3/-4			HR-7/-8		
	Term <i>a</i>	Term <i>b</i>	Term <i>c</i>	Term <i>a</i>	Term <i>b</i>	Term <i>c</i>
<i>t</i> =0	16	0	0	25	0	0
<i>t</i> =1.08	16	0	10	25	0	5
<i>t</i> =inf.	16	0	48	25	0	45
	$a(t) = 16$	$b(t) = 0$	$c(t) = 15 - \exp(-0.0636t+2.7080)$	$a(t) = 25$	$b(t) = 0$	$c(t) = 8 - \exp(-0.4338t+2.0794)$

Table 3. Values of terms *a*, *b*, and *c* in the model of diagnostic biomarker shift as a function of time. IPL values are absolute abundance (ng/g). 16S rRNA gene values are relative abundance. For the 16S rRNA gene biomarkers, multiple OTUs of some taxa (e.g., *Helicobacteraceae*) were identified. Biomarkers characteristic of low-activity conditions are given in blue; biomarkers characteristic of active conditions are given in red. Bold and italicized text indicate archaeal and bacterial biomarkers, respectively. Values at *t*=0 are medians from the native-active carbonates. Values at *t*=1.08 are median values from the transplant-to-low-activity carbonates. Values at *t*=infinity are the median values from the native-low-activity carbonates. Low-activity-type biomarkers increase in abundance with time; active-type biomarkers decrease in abundance with time. Three criteria were used to identify characteristic biomarkers for this analysis (see main text):

- (i) In order to qualify as an active-type IPL, Q1 of the IPL among the native-active carbonates must be greater than Q3 of the IPL among the native-low-activity carbonates. In order to qualify as a low-activity-type IPL, Q3 of the IPL among the native-active carbonates must be less than Q1 of the IPL among the native-low-activity carbonates.
- (ii) The median of the IPL among the transplanted (active to low-activity) carbonates must be between the medians of the IPL among the native-active and native-low-activity carbonates.
- (iii) In order to qualify as an active-type IPL, the median of the IPL among native-active carbonates must be greater than 4.43 ng/g in concentration. In order to qualify as a low-activity-type IPL, the median of the IPL among native-low-activity carbonates must be greater than 4.43 ng/g in concentration. For this criterion, the value of 4.43 ng/g was chosen because it is 1% of the median total IPL concentration for all native and transplantation carbonates in this study.

In order to identify key 16S rRNA genes of interest, we employed the same criteria with one modification on the third criterion in order to account for the relative abundance nature of the 16S rRNA gene dataset: rather than a cutoff value of 4.43 ng/g (irrelevant to the 16S rRNA gene data), we applied a cutoff of 1% relative abundance. After identifying specific biomarkers (Fig. 7), we applied a log-linear approach in order to generate biomarker-specific models (Fig. 8; Table 3).

Lipid Biomarkers		Characteristic of Active Seep Environments		
		PE-DAG-C30:1	PE-DAG-C34:2	PC-DAG-C34:2
Time (Years)	2G-GDGT	5.2461	13.6130	20.4486
<i>t</i> =0	2.3761	14.1018	10.4892	48.3031
<i>t</i> =1.08	2.9358	8.3764	10.8297	16.1597
<i>t</i> =inf.	32.9653	1.6326	0.9942	0.0000

16S rRNA Biomarkers		Characteristic of Low-Activity Seep Environments			Characteristic of Active Seep Environments		
		ANME1b	MBGD	JTB255	Broccidiaceae	Helicobacteraceae	Helicobacteraceae
Time (Years)	MG1	0.0193	0.0007	0.0002	0.0021	0.0796	0.0150
<i>t</i> =0	0.0193	0.0007	0.0002	0.0021	0.0796	0.0173	0.0144
<i>t</i> =1.08	0.0727	0.0018	0.0004	0.0009	0.0048	0.0117	0.0099
<i>t</i> =inf.	0.1581	0.0140	0.0118	0.0103	0.0104	0.0002	0.0002

3.8 FIGURES

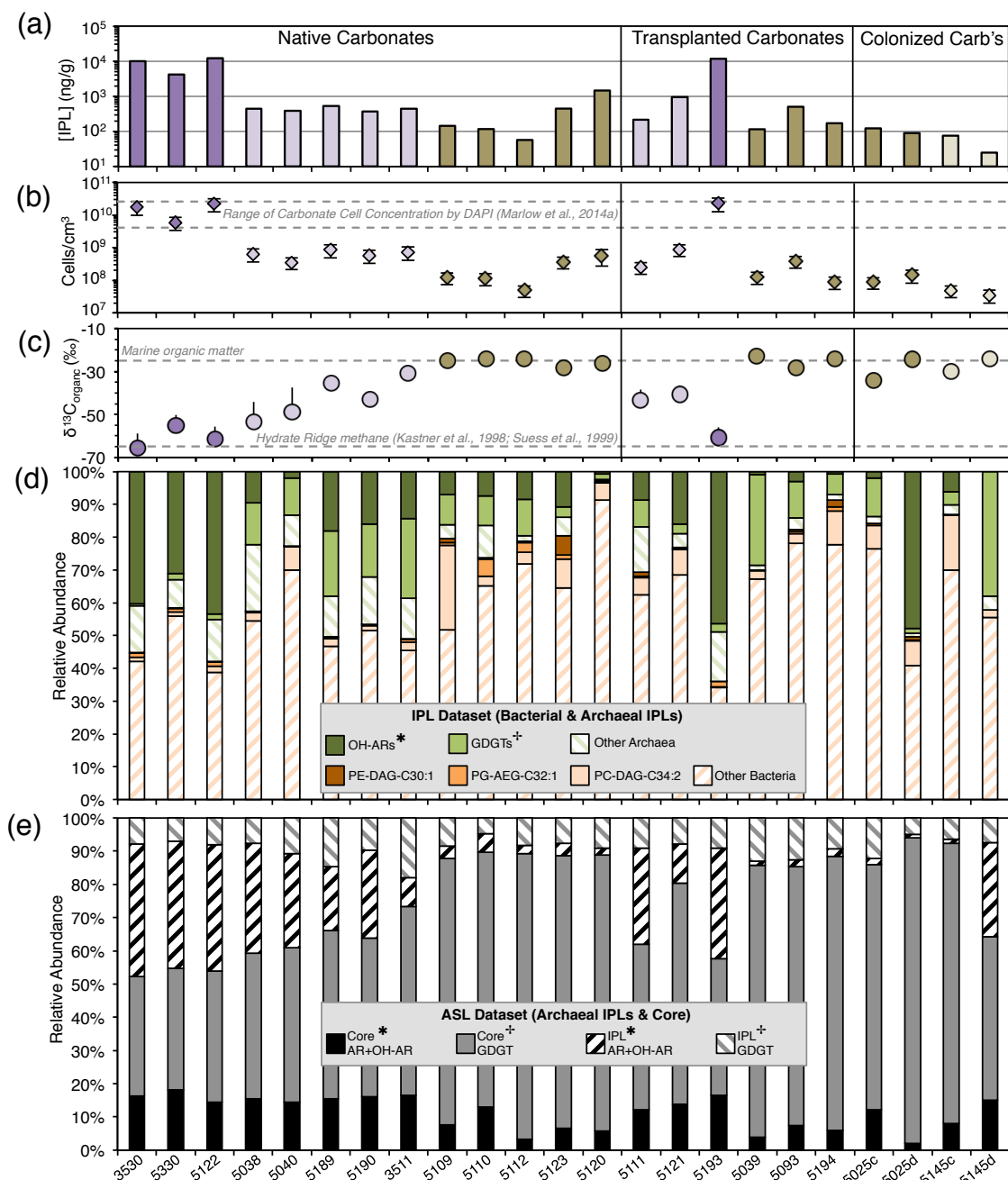


Fig. 1: Lipid and geochemical data from authigenic carbonates at Hydrate Ridge. (a) Summed quantitative bacterial and archaeal IPL concentration is reported in ng IPL per g dry carbonate powder. Purple and brown colors represent aragonitic and calcitic/dolomitic mineralogy groups, respectively. The dark and light color shading indicate active and low-activity seep stations, respectively. For transplant carbonates, these shadings represent the seep station from which the rocks were transplanted (their origin). These colors and shadings also apply in panels (b) and (c). In panel (b), IPL concentrations are converted to cells/cm³ using multiple conversion metrics (see Supplemental Text for calculation details and assumptions). As a comparison, horizontal dashed gray lines indicate the cell concentration range determined for methane seep carbonates by direct DAPI cell counts in Marlow et al., 2014a. (c) $\delta^{13}C$ for carbonate-hosted microorganisms ($\delta^{13}C_{org}$) for each sample, with instrumental uncertainty represented by vertical black lines. (d) Relative abundance IPL profile for each carbonate sample, with IPLs putatively associated with ANME-1 (summed GDGTs) and ANME-2 (summed OH-ARs) identified by superscript symbols (+ and *, respectively; also applied in (e)). Green and orange bars represent archaeal and bacterial IPLs, respectively. (e) Relative abundance profiles of the Archaeal Semiquantitative Lipids (ASL) dataset, with both archaeal IPL (striped) and core lipids (filled) identified.

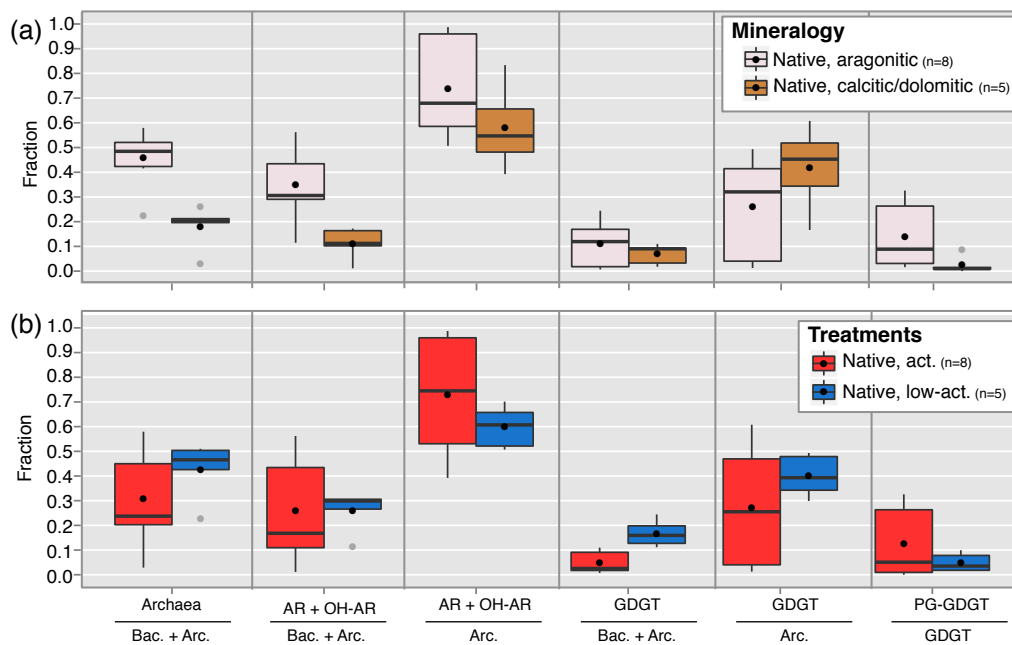


Fig. 2: Specific IPL ratios of native carbonates. (a) Samples are binned according to bulk mineralogy, (b) Samples are binned according to seep activity. Median values are given by the horizontal black line, with the colored boxes encompassing the first through third quartiles of the data. Upper and lower whiskers denote the highest and lowest data points within 1.5 times the interquartile (Q_{75} minus Q_{25}) range. Any data points outside this range are identified by gray circles. Mean values are identified by black circles, but the non-normal distribution of IPL abundances among seep carbonates implies that medians are a better statistical measure than means for this dataset. All ratios are calculated from quantitative bacterial and archaeal IPL data. The sum of AR and OH-AR (all archaeols and all hydroxyarchaeols) was used to infer the contribution of ANME-2 among in carbonate samples (Table S3). The ratio of all GDGT IPLs was calculated to infer the contribution of ANME-1 among carbonate samples. The ratio of $PG-GDGT_{All}$ (PG-GDGT, G-GDGT-PG, and 2G-GDGT-PG) over total GDGTs was calculated as a proxy for active ANME-1 biomass as has previously been suggested (Kellermann et al., 2016; Yoshinaga et al., 2015).

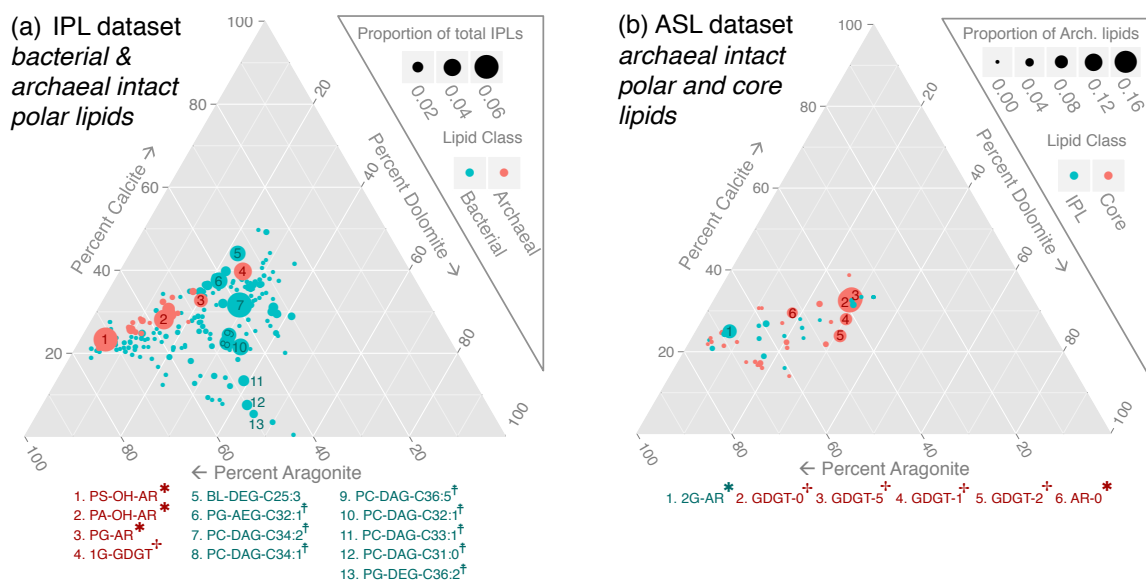


Fig. 3: Ternary diagrams of lipid biomarker data associated with carbonate mineralogy. (a) Bacterial and archaeal IPL data and (b) archaeal IPL and core lipid data according to mineralogical distributions. Only native-active samples were included in order to isolate the affect of mineralogy and avoid any influences of experimental treatment or seep activity. To calculate the percent association of each lipid with each mineralogy, for each carbonate the relative abundance of the lipid was divided into weighted proportions according to the mineralogy of the sample. These proportions were then summed for each mineralogy across all samples. Selected lipids are identified in (a) and (b) as dominant lipids in the respective datasets and identified below the plots. Bacterial non-isoprenoidal ether- and ester-bound lipids with a mass range of between 30 and 36 carbons (identified in (a) with double cross) would be consistent with SRB, according to numerous and extensive methane seep environmental characterizations (e.g., Rossel et al., 2008). As in Fig. 1d-e, archaeal lipids likely associated with ANME-1 and ANME-2 are denoted with a single cross and asterisk, respectively.

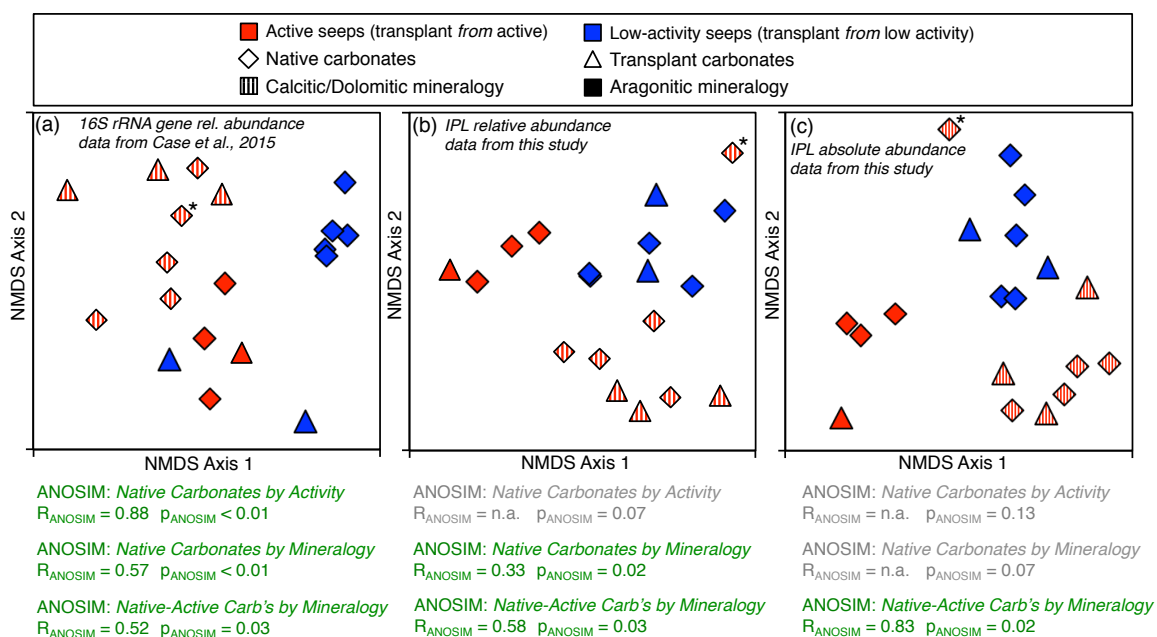


Fig. 4: Non-metric multidimensional scaling ordinations. (a) seep carbonate-associated 16S rRNA gene biomarkers from Hydrate Ridge, for the same set of samples from which lipids were extracted in this study (stress = 0.16; data published in Case et al., 2015); (b) Relative abundance IPL profiles from this study (stress = 0.15); (c) Absolute abundance IPL profiles from this study (stress = 0.07). The native-active carbonate in the upper portion of (b) and (c) is sample #5120 (marked with an asterisk in (a) also), which has previously been determined to host a microbial community anomalously high in ANME-1 compared to other native-active carbonates (Marlow et al., 2014a; Case et al., 2015). ANOSIM test results are given in green where statistically significant and in gray where statistically insignificant.

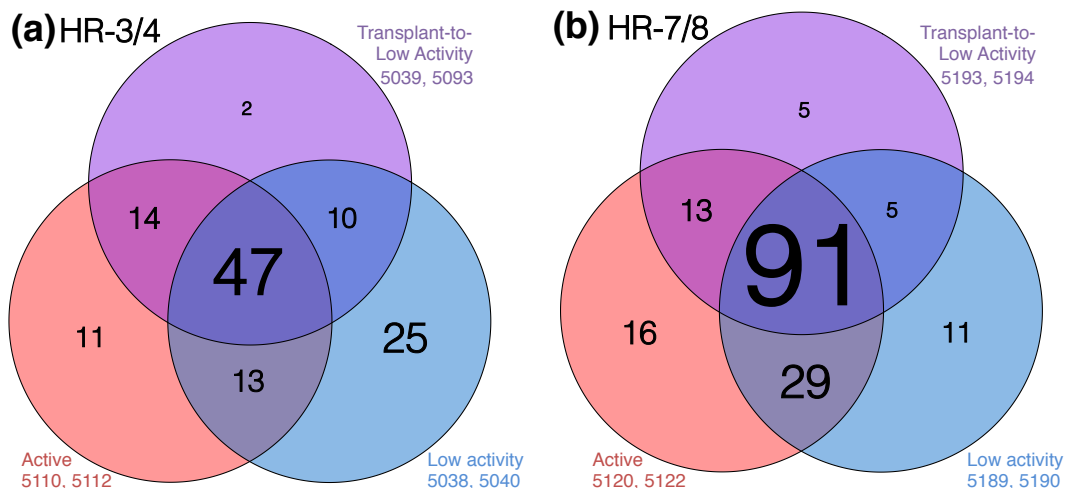
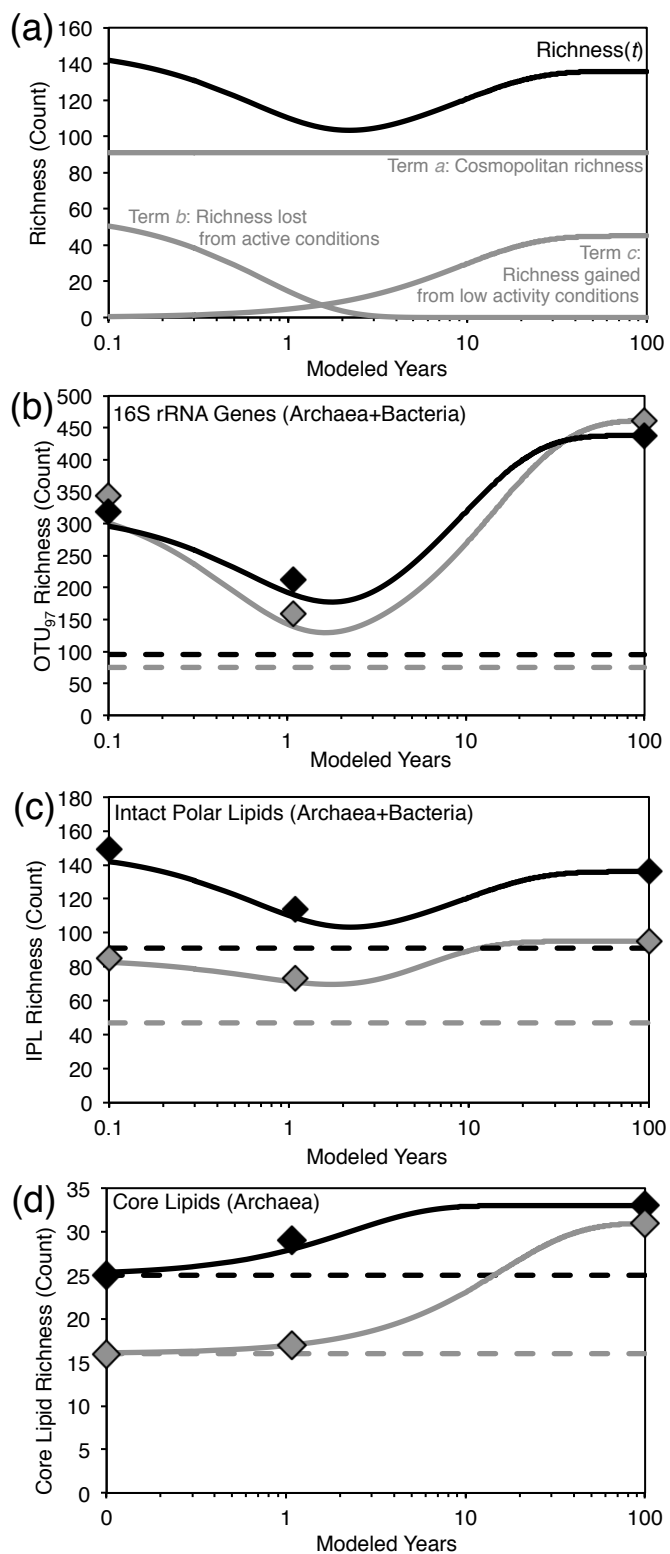


Fig. 5: Venn diagrams of lipid richness for parallel transplant experiments. (a) Transplant experiments at the paired sites HR-3 (active) and HR-4 (low-activity), (b) transplant experiments at the paired sites HR-7 (active) and HR-8 (low-activity). For each field of the Venn diagram, two duplicate samples were included (sample numbers are given in the figure). In order for a lipid to count as “present” for this presence/absence analysis, it must have been recovered from both replicates. This conservative requirement took advantage of having carbonates representing duplicate *in situ* treatment conditions on the seafloor. Although transplant-to-active experiments were conducted, they were not included in this analysis due to low replicate number. In each field of the Venn diagrams, text size is proportional to value. Twenty-eight percent ($n=(11+13)/(11+13+14+47)$) in panel (a) and 30% ($n=(16+29)/(16+29+13+91)$) in panel (b)) of the IPLs present in native-active carbonates were lost after 13 months of seep dormancy in transplanted carbonates. After 13 months, only 11% ($n=10/(10+25+13+47)$) in panel (a) and 4% ($n=5/(5+11+29+91)$) in panel (b)) of the IPLs present in native-low-activity carbonates have appeared in the transplant carbonates.

Fig. 6: Model of richness over time for 16S rRNA gene, IPL, and core lipid biomarkers. (a) Demonstration of Terms *a*, *b*, and *c* in Equation 1, (b) 16S rRNA gene richness, (c) IPL (bacteria+archaea) richness, and (d) core archaeal lipid richness. In (b-d), the model is given by the curved solid line and the data points used to generate the model are given by diamonds. The dashed lines represent the core cosmopolitan biomarker richness. Results from parallel *in situ* experiments at HR-3/4 (gray) and HR-7/8 (black) are given. The model is not *a priori* required to intercept each data point. A higher number of data points could increase predictive accuracy of the model and/or reveal highly complex temporal dynamics not currently observed. A maximum model length of 100 years was chosen because by that time, little remaining change in biomarker richness occurred. See Supplemental Text for modeling results from other sample permutations.



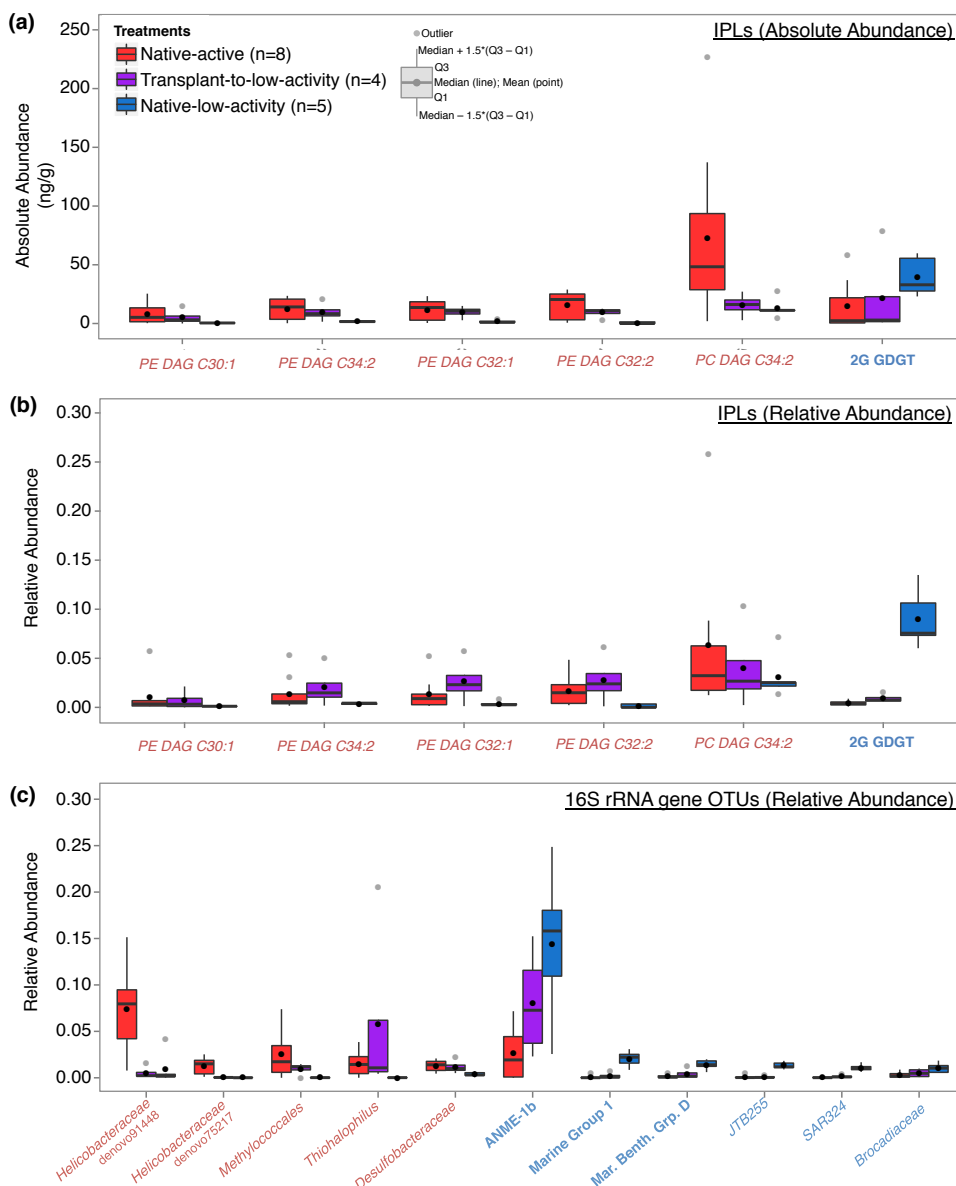


Fig. 7: Box plots of biomarkers identified as characteristic of active or low-activity seep conditions. Absolute abundances of IPL biomarkers are given in (a), with relative abundances of the same biomarkers given in (b). Panel (c) gives relative abundances of 16S rRNA gene biomarkers. Three criteria were used to identify characteristic biomarkers for this analysis (see main text):

- (i) In order to qualify as an active-type IPL, Q1 of the IPL among the native-active carbonates must be greater than Q3 of the IPL among the native-low-activity carbonates. In order to qualify as a low-activity-type IPL, Q3 of the IPL among the native-active carbonates must be less than Q1 of the IPL among the native-low-activity carbonates.
- (ii) The median of the IPL among the transplanted (active to low-activity) carbonates must be between the medians of the IPL among the native-active and native-low-activity carbonates.
- (iii) In order to qualify as an active-type IPL, the median of the IPL among native-active carbonates must be greater than 4.43 ng/g in concentration. In order to qualify as a low-activity-type IPL, the median of the IPL among native-low-activity carbonates must be greater than 4.43 ng/g in concentration. For this criterion, the value of 4.43 ng/g was chosen because it is 1% of the median total IPL concentration for all native and transplantation carbonates in this study.

In order to identify key 16S rRNA genes of interest, we employed the same criteria with one modification on the third criterion in order to account for the relative abundance nature of the 16S rRNA gene dataset: rather than a cutoff value of 4.43 ng/g (irrelevant to the 16S rRNA gene data), we applied a cutoff of 1% relative abundance. After identifying specific biomarkers (Fig. 7), we applied a log-linear approach in order to generate biomarker-specific models (Fig. 8; Table 3).

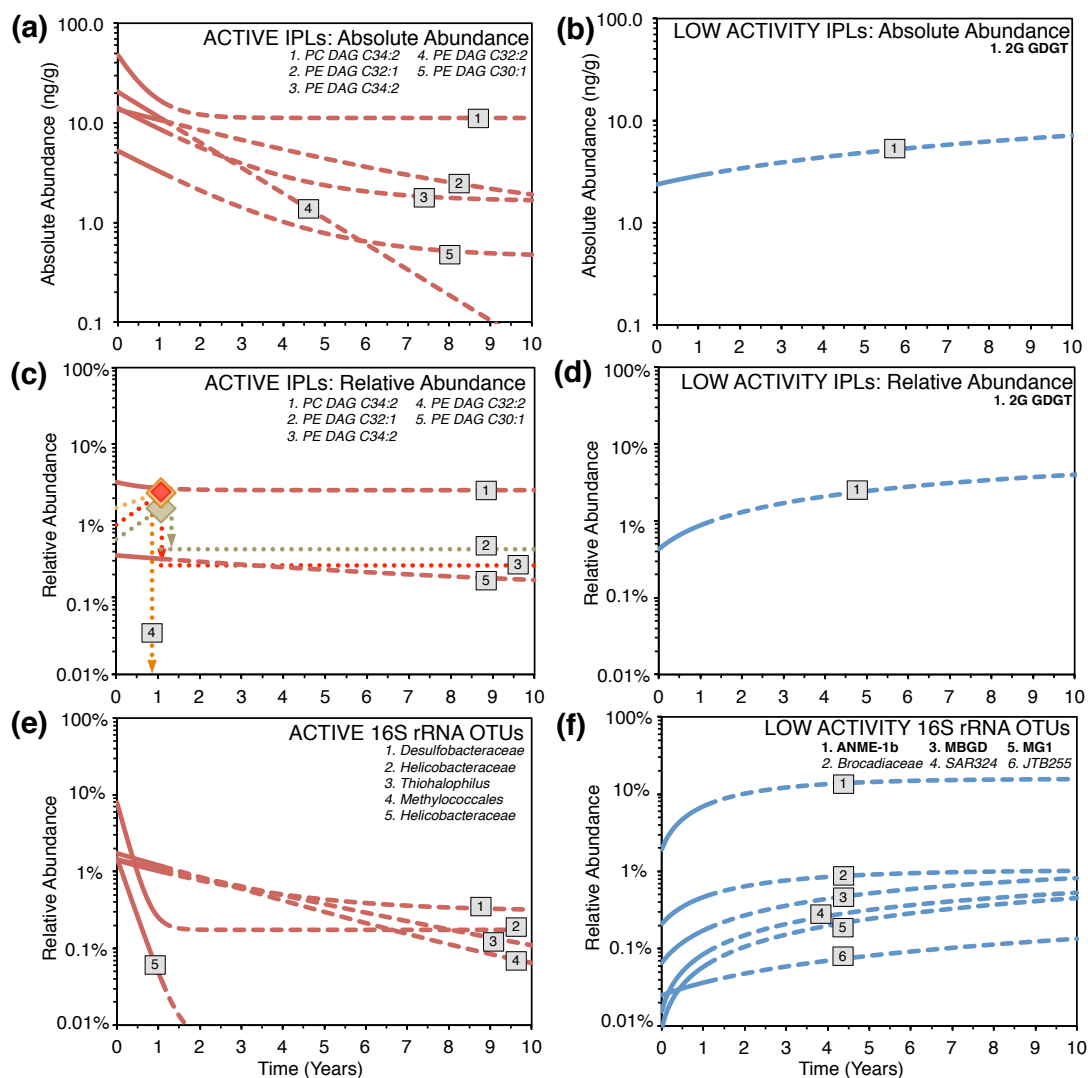


Fig. 8: Model of specific biomarker turnover for IPL and 16S rRNA gene biomarkers. Panels (a) and (b) give absolute abundances of IPLs identified as characteristic of active or low-activity seepage, respectively. Panels (c) and (d) give the same IPLs in relative abundance. Panels (e) and (f) show 16S rRNA gene OTUs identified as diagnostic of low-activity conditions. See main text and caption to Fig. 7 for description of criteria used to identify active-type and low-activity-type biomarkers. Biomarkers identified in italics are bacterial, biomarkers in bold are archaeal. Red lines indicate active-type biomarkers; blue lines indicate low-activity-type biomarkers. In all panels, solid model lines represent the timescale of the transplantation experiments (13 months), and the dashed lines represent extrapolation beyond 13 months. In panel (c), dotted lines indicate behavior of IPLs that demonstrated first a rise and then a drop in relative abundance. This behavior was not compatible with the modeling algorithm in which the median values at $t=1.08$ derived from the transplant carbonates must be between the median values from the native-active and native-low-activity carbonates, and therefore dotted lines are used to demonstrate behavior rather than the modeled solid and dashed lines elsewhere in the figure. In panels (a) and (c), IPL #4 (*PE-DAG-C32:2*) goes to zero at infinite time (i.e., the IPL is not observed in the native-low-activity carbonates).

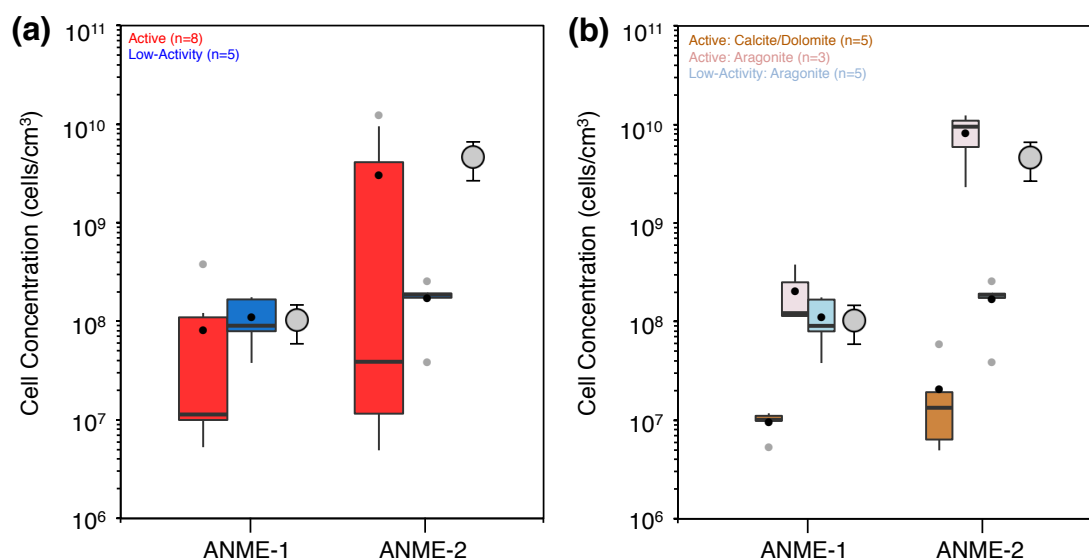


Fig. 9: Calculated cell concentrations of ANME-1 and ANME-2. Cell concentrations from seep carbonates in this study were calculated by applying conversion factors for the density of carbonate and the specific IPL content of bacterial and archaeal cells (see Supplemental Text for details). Panel (a) gives data for seep carbonates parsed by seep activity in red and blue box plots indicating active and low-activity seep conditions, respectively. Panel (b) gives data for seep carbonates parsed by both activity and mineralogy. Gray circles in both panels indicate average and standard deviations of calculated cell concentrations from reported literature values of active seep shallow sediments at Hydrate Ridge, OR (See main text for additional details; Boetius et al. 2000; Treude et al. 2003; Knittel et al. 2005; Marlow et al. 2014a). Box plots parameters are given in the caption to Fig. 2 and sketched schematically in Fig. 7a.

3.9 SUPPLEMENTAL MATERIAL: TEXT

3.9.1 MINERALOGICAL DETERMINATION BY X-RAY DIFFRACTION

In order to quantify the proportions of aragonite, calcite, and dolomite within our samples, we created a standard set of carbonate powder mixes composed of powders from pure carbonate samples. Through XRD analysis of these standards, we could use empirical data to develop a quantitative algorithm for calculating carbonate composition in our environmental samples. This approach follows naturally from previous studies which used the ratio of diagnostic calcite and dolomite peaks to determine calcite/dolomite mixing ratios in carbonate samples (Tennant and Berger 1957; Bergmann 2013). However, we expand this approach to also include aragonite inter-mixing. Recent studies have probed aragonite, calcite, and dolomite presence in seep carbonate samples, but have not reported quantitative mixing fractions of the morphologies (Marlow et al. 2014b; Case et al. 2015).

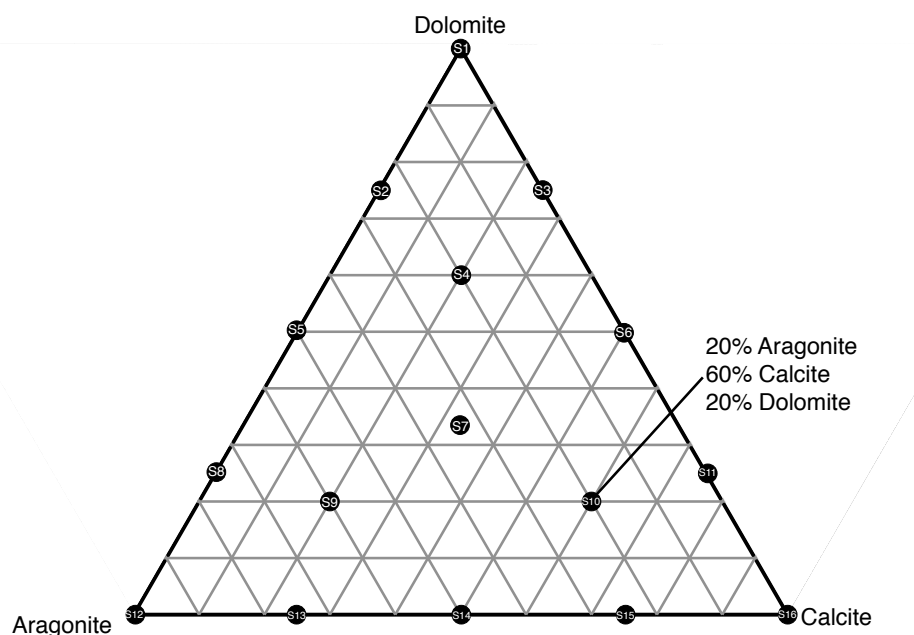


Fig. 3.9-1. Mixing fractions of 16 standard powders for developing carbonate bulk XRD quantitation.

For each morphology, we chose as diagnostic for the most dominant peak in pure-powder XRD spectra (S1, S12, and S16): aragonite ($26.3^\circ 2\theta$), calcite ($29.5^\circ 2\theta$), and dolomite ($31.0^\circ 2\theta$):

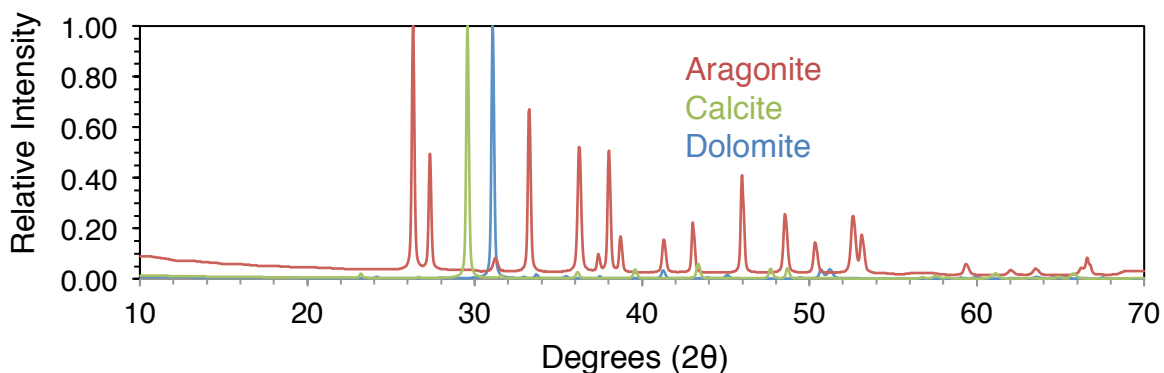


Fig. 3.9-2. Bulk XRD spectra of pure powders of aragonite, calcite, and dolomite.

By quantifying the area of the diagnostic peak for each morphology, we were able to calculate simple mixing fractions to develop a quantitative framework. Firstly, we calculate the mixing fraction of aragonite (f_{arag}) in each standard powder and compare to the known concentration ($\%_{\text{arag}}$):

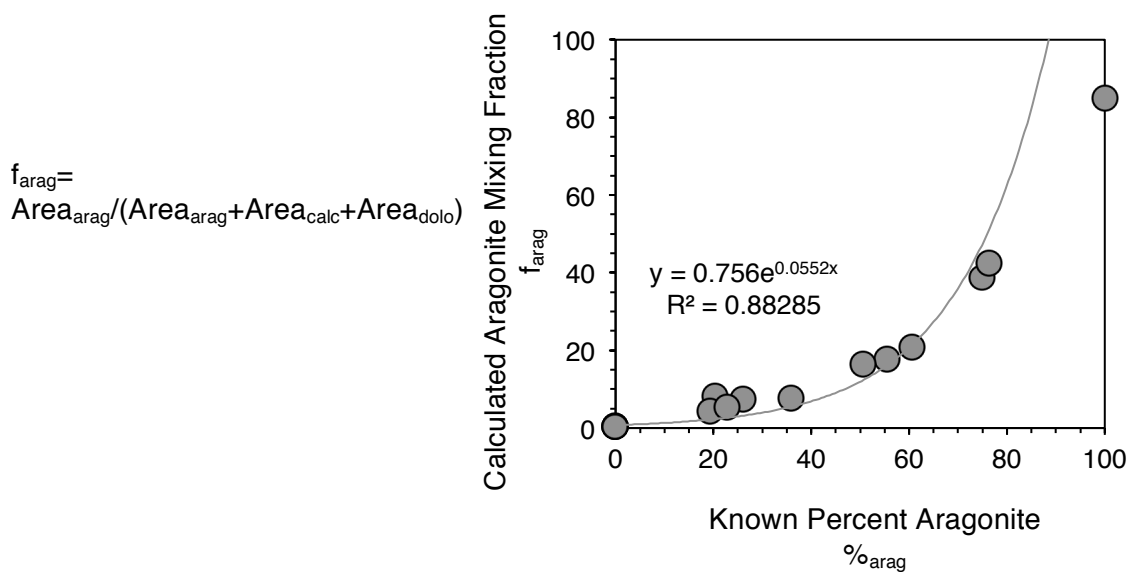


Fig. 3.9-3. Calibration curve for quantifying percent aragonite in a carbonate sample of mixed mineralogy with aragonite, calcite, and dolomite.

To a good degree, we have thus established an empirical relationship to determine the percent aragonite in a sample based on the mixing ratio of the aragonite peak at $26.3^\circ 2\theta$. We can subtract this percent aragonite from 100%, and the remainder can be assigned to calcite and dolomite according to two-endmember mixing as has been described previously (Tennant and Berger 1957; Bergmann 2013):

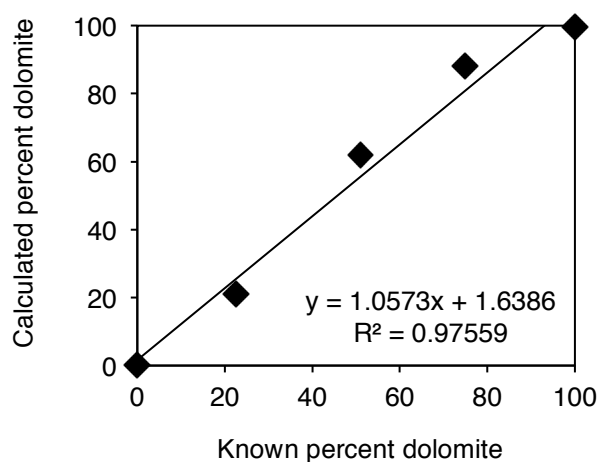


Fig. 3.9-4. Verification of accuracy of calculating mixing fractions of calcite and dolomite in standard samples of only calcite and dolomite composition.

Finally, we can compare our algorithm to the known fractions of aragonite, calcite, and dolomite in each of the 16 standard mixtures:

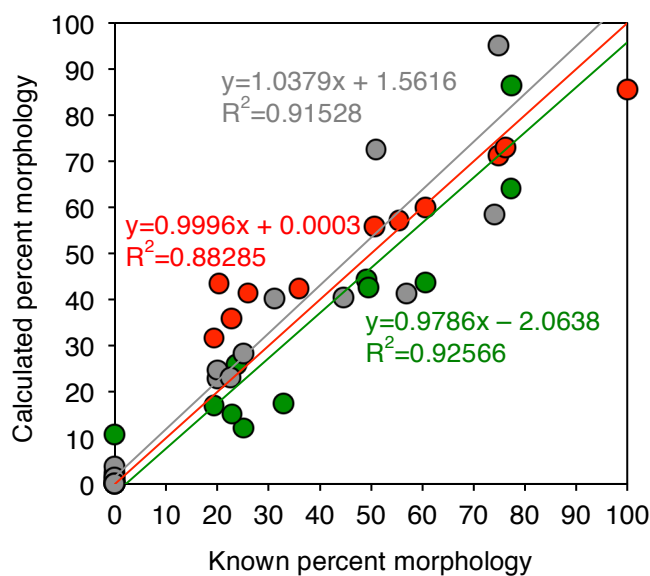


Fig. 3.9-5. Verification of our full quantitation pipeline on the suite of 16 standard powders. Red=Aragonite, Gray=Dolomite, Green=Calcite.

There is substantial scatter away from a 1:1 line among the data points. Ultimately, this empirical algorithm is able to quantitatively estimate carbonate morphology mixing fractions to within $\pm 15\%$. Although the uncertainty is relatively high, we are able to apply this algorithm to our environmental samples to get an estimate of carbonate composition.

Plotting our environmental samples on a ternary diagram, we see that the carbonates fall into two categories: aragonitic (red) and calcitic/dolomitic (teal). The aragonitic samples are $>60\%$ aragonite, whereas calcitic/dolomitic samples are $<60\%$ aragonite. Manual analysis of XRD spectra for every environmental sample confirmed the binning into aragonitic and calcitic/dolomitic bins made logical sense.

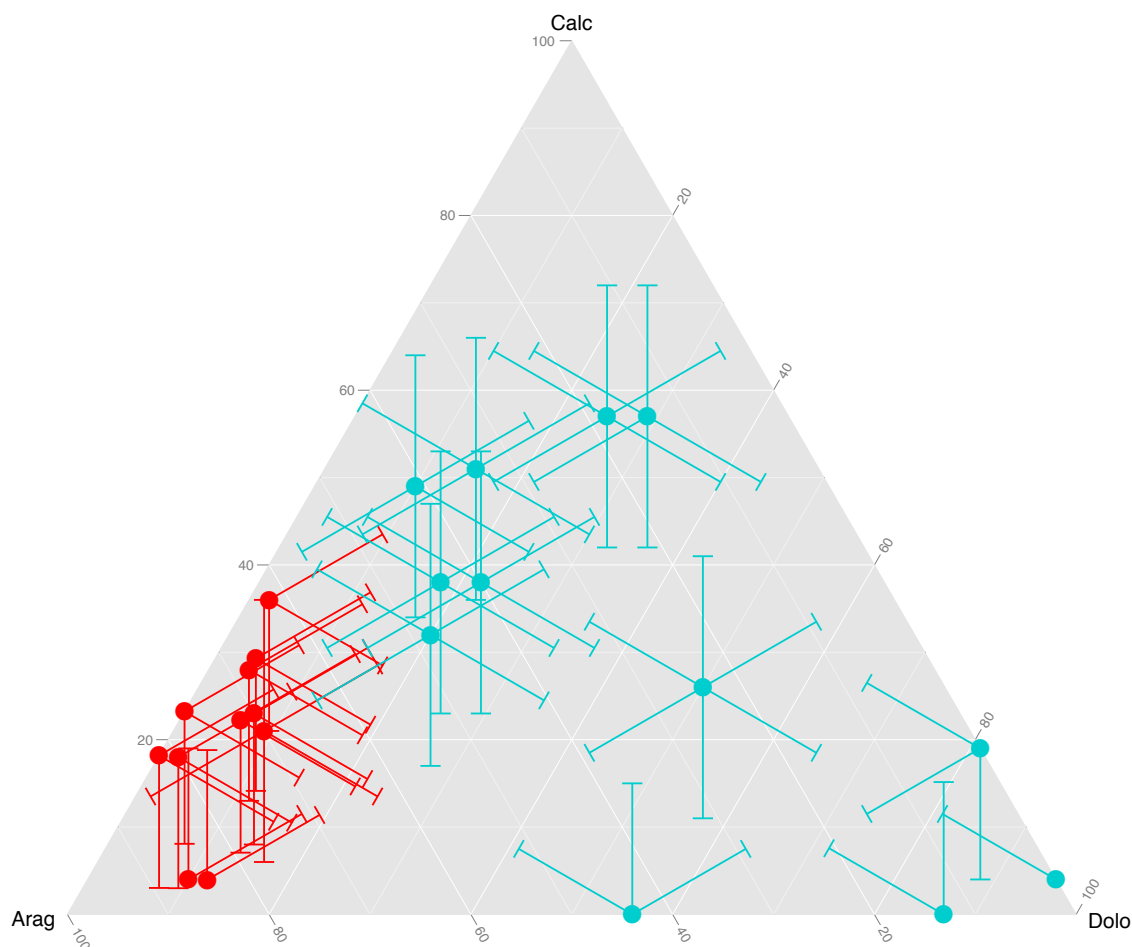
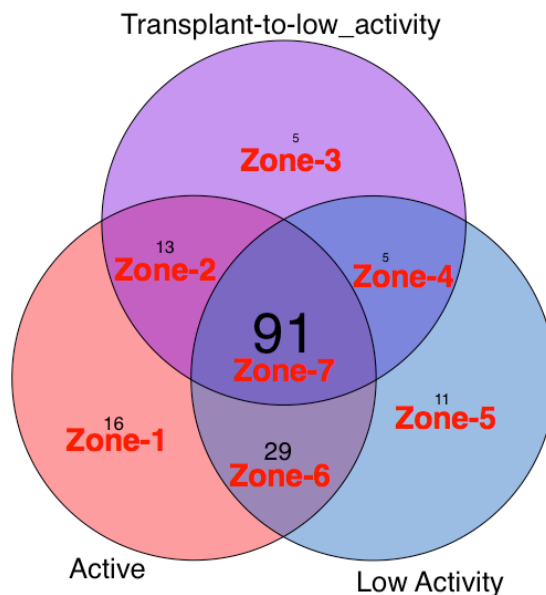


Fig. 3.9-6. Ternary diagram of environmental samples according to their mixing proportions of aragonite, calcite, and dolomite.

3.9.2 DESCRIPTION OF RICHNESS MODELING APPROACH

**Zone Descriptions**

Zone-1: Richness lost after 13 months of seep quiescence, never to be re-gained.

Zone-2: Richness retained after 13 months of seep quiescence, later to be lost permanently.

Zone-3: Richness temporarily gained after 13 months of seep quiescence, later to be lost permanently.

Zone-4: Richness gained after 13 months of seep quiescence, to be permanently kept.

Zone-5: Richness not gained yet after 13 months of seep quiescence, but later to be permanently acquired.

Zone-6: Richness loss after 13 months of seep quiescence, but later to be regained permanently.

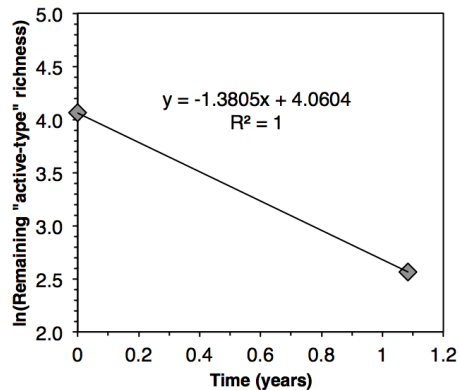
Zone-7: Richness never lost nor gained; cosmopolitan richness.

Modeling Richness Loss

At $t=0.00$ yr, all richness that will be lost is represented by Zones 1, 2, and 6 (e.g., $n=58$).

At $t=1.08$ yr, Zones 1 and 6 are already lost and only Zone 2 remains (e.g., $n=13$).

Assuming the amount of “active-type” richness remaining is a log-linear function with time, an exponential model of decay results as defined by two data points: $(0.00, \ln(58))$ and $(1.08, \ln(13))$.



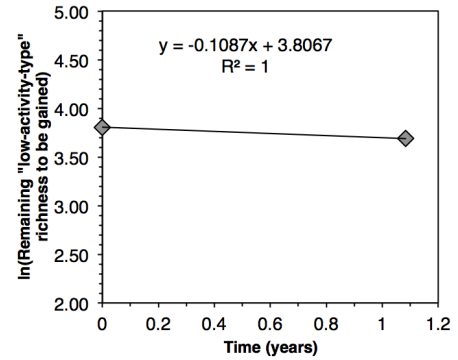
Modeling Richness Gain

Richness gain is modeled according to the amount of richness remaining to be gained.

At $t=0.00$, the richness that remains to be gained is represented by Zones 4, 5 and 6 (e.g., $n=45$).

At $t=1.08$, the richness that remains to be gained is represented by Zones 5 and 6 (e.g., $n=40$).

Assuming the amount of “low-activity-type” richness remaining to be gained is a log-linear function with time, an exponential model of decay results as defined by two data points: $(0.00, \ln(45))$ and $(1.08, \ln(40))$.



Putting the Model Together

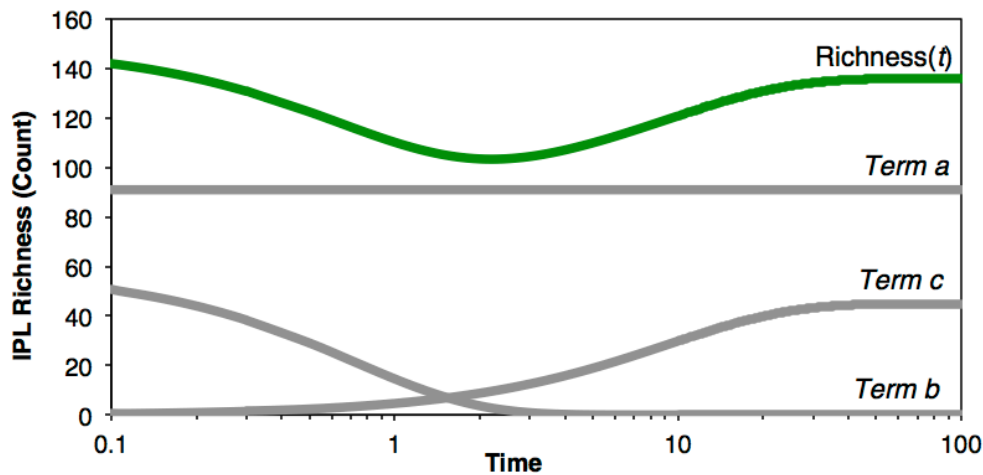
At any given time t , the amount of richness can be defined as the sum of three terms:

- a) The constant richness never lost nor gained (Zone 7; “cosmopolitan richness”).
- b) The richness remaining from the “active-type” environment.
- c) The richness gained from the “low-activity-type” environment.

Term a, in this example, has a value of 91. *Term b* is a function of t defined in the first plot above. *Term c* is not quite the equation defined in the second plot above. The plot defines the amount of richness remaining to be gained, while we want to sum the amount of richness that has already been gained. This is achieved by subtracting the amount of richness remaining to be gained from the ultimate “low-activity-type” richness, in this example, 45.

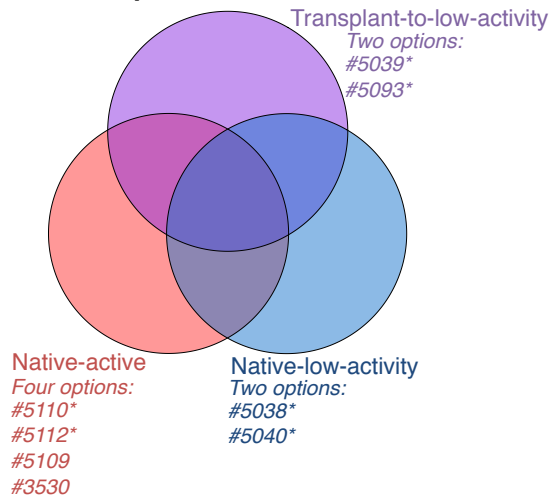
The equation is thus:

$$\text{Richness}(t) = \begin{matrix} \text{Term } a \\ 91 \end{matrix} + \begin{matrix} \text{Term } b \\ \exp(-1.3805t + 4.0604) \end{matrix} + \begin{matrix} \text{Term } c \\ (45 - \exp(-0.1087t + 3.8067)) \end{matrix}$$

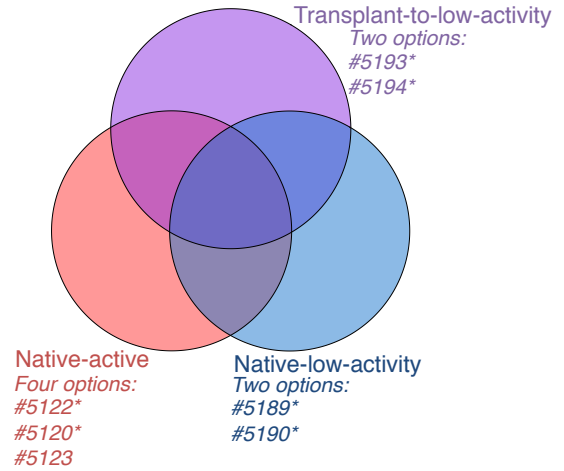


Because richness as defined here (presence/absence count) is highly sensitive to the number of samples examined (discovery opportunity), we require the number of samples representing each category to be equal (in Fig. 5 of the main text, two samples are chosen for each of the native-active, transplant-to-low-activity, and native-low-activity categories). In order to test whether sample choice had a significant impact on model output, we performed the model with all possible combinations of samples representing each category (See figure on next page). Overall the model behavior is independent of the specific samples chosen, especially for 16S rRNA gene and IPL biomarkers. For core lipids, in particular at the paired HR-3/4 stations, the specific sample-sample combinations in some instances made a significant impact on the model results. This was due to some sample-sample pairs indicating “active-site-specific” core lipids, while other sample-sample pairs indicated zero “active-site-specific” core lipids (Zone 1 in the Venn diagram described above). Thus, the core lipid modeling results are the most tentative although we note that between HR-3/4 and HR-7/8, only 2 out of 9 permutations yielded the odd model structure. Seven out of nine were congruent with the “richness increase” trend presented in Fig. 6 of the main text.

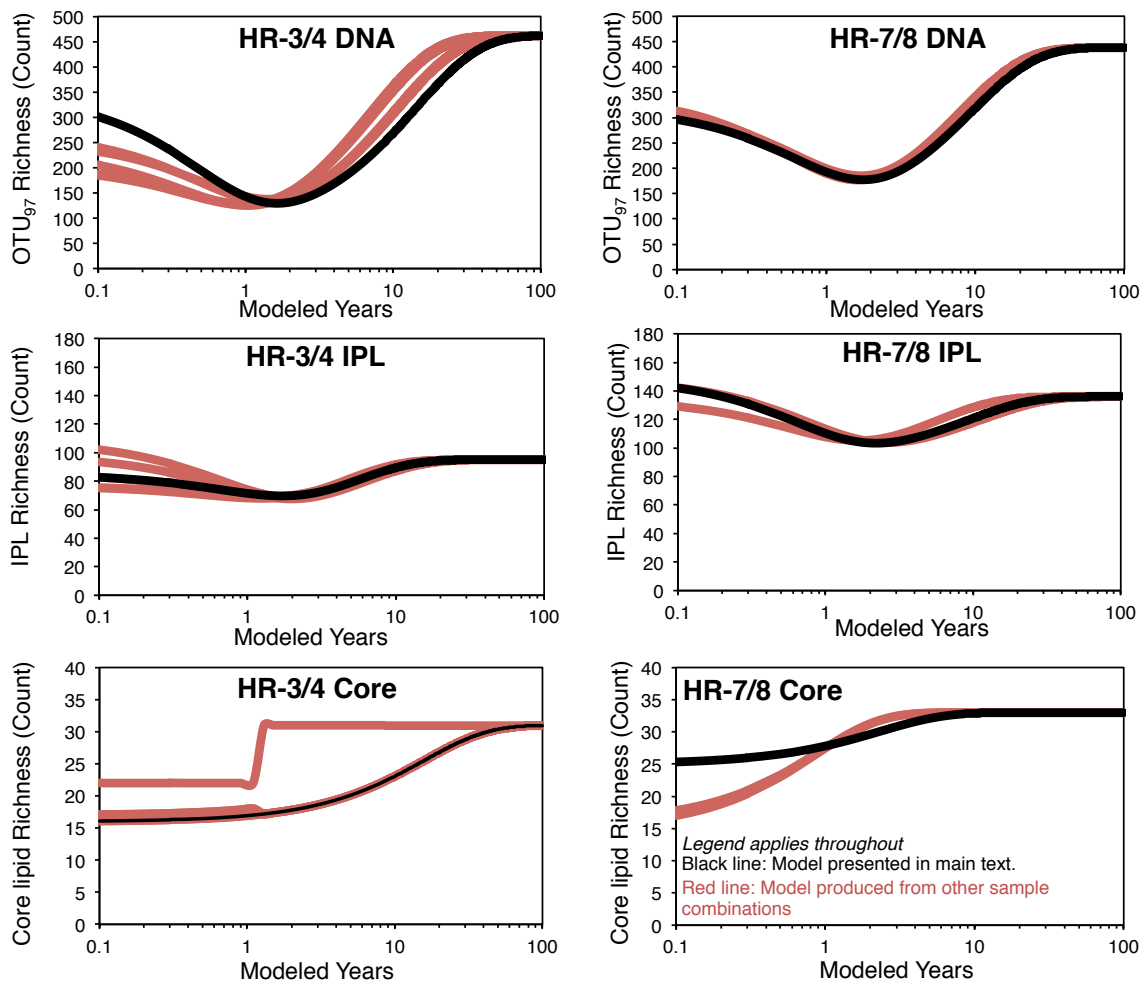
HR-3/4: Requiring two samples per category yields 6 permutations



HR-7/8: Requiring two samples per category yields 3 permutations



Samples with * were used for presentation in the main text and were chosen to match the samples chosen in Case et al. (2015) mBio, which were chosen randomly.



3.9.3 CONVERTING ng/g TO cells/cm³

IPL concentrations in this study were well characterized in ngIPL per g_{dry carbonate}. In order to compare to other studies (e.g., Marlow et al. 2014a), this value is best converted into cells per cubic centimeter of carbonate. In order to perform this conversion, we applied the following assumed values:

Constants:

$\rho_{\text{aragonite}} = 2.93 \text{ g/cc}$	
$\rho_{\text{calcite}} = 2.71 \text{ g/cc}$	
$\rho_{\text{dolomite}} = 2.83 \text{ g/cc}$	
Porosity of seep carbonates = 16.3%	[average value from Marlow et al. 2014a]
Cellular IPL weight A = 18.3 fgIPL/cell	[Zink et al. 2008; derived for marine subsurface bacteria]
Cellular IPL weight B = 4.9 fgIPL/cell	[Simon and Azam 1989; theoretical calculation for marine bacteria]
Cellular IPL weight C = 0.58 fgIPL/cell	[Meador et al. 2014; empirical from archaeal <i>Thermococcus kodakarensis</i> pure culture]
Cellular IPL weight D = 1.4 fgIPL/cell	[Lipp et al. 2008; theoretical calculation for archaeal cells]

Based upon these values, four calculations were performed in order to generate estimates of cell density (cells/cm³) from IPL concentrations (ng/g). The density of each carbonate was inferred by applying the densities of each CaCO₃ morphology with the weighted mineralogical composition of each rock, and accounting for the average porosity of seep carbonates. Conversion of IPL abundance (ng) to cellular abundance was completed separately for archaeal and bacterial IPLs, using the empirical and theoretical values given above. Thus, four estimates of cell concentration were generated:

- Estimate 1: Bacterial IPLs converted with Zink et al., 2008 value; archaeal IPLs converted with Meador et al., 2014 value.
- Estimate 2: Bacterial IPLs converted with Zink et al., 2008 value; archaeal IPLs converted with Lipp et al., 2008 value.
- Estimate 3: Bacterial IPLs converted with Simon & Azam, 1989 value; archaeal IPLs converted with Meador et al., 2014 value.
- Estimate 4: Bacterial IPLs converted with Simon & Azam, 1989 value; archaeal IPLs converted with Lipp et al., 2008 value.

These calculations result in highly similar estimates of seep carbonate cell density as a function of recoverable IPL concentrations. Therefore, the results are reported as average and standard deviation of the four calculations in Fig. 1b.

3.10 SUPPLEMENTAL MATERIAL: TABLES

Table S1. Concentrations of polar lipids were corrected using response factors based on commercial or purified standards (as listed below) to account for differences in ionization during HPLC-ESI-MS.

#	Standard	Source	Polar Lipids
1	G-GDGT 0	Zhu et al. (2013)	G-GDGT(0-5)
2	2G-GDGT 0	Zhu et al. (2013)	2G-GDGT(0-5)
3	G-GDGT-PG	Matreya LLC, PA, USA	PG-GDGT(0-4)-G/2G/PG
4	G-AR	Zhu et al. (2013)	G-AR/OH-AR
5	2G-AR	Zhu et al. (2013)	2GAR/OH-AR
6	PE-AR	Avanti Polar Lipids Inc., USA	PG/PI/PE/PS-AR*
7	C _{21:0} /C _{21:0} -PC	Avanti Polar Lipids Inc., USA	PC/PI (DAG/AEG/DEG)
8	Glucosylceramide	Avanti Polar Lipids Inc., USA	PE/PG/PI - Sphingolipids
9	C _{16:0} /C _{16:0} -DGTS	Avanti Polar Lipids Inc., USA	BL/OL
10	C _{16:0} /C _{16:0} -PE	Avanti Polar Lipids Inc., USA	PE (DAG/AEG/DEG)
11	C _{16:0} /C _{16:0} -PDME	Avanti Polar Lipids Inc., USA	PME (DAG/AEG), PDME (DAG)
12	2C _{18:1} /2C _{18:1} -CL	Avanti Polar Lipids Inc., USA	CL/monolysyl CL
13	C _{16:0} /C _{16:0} -PG	Avanti Polar Lipids Inc., USA	PG (AEG/DEG)

1. monoglycosyl glycerol dibiphytanyl glycerol tetraether; 2. diglycosyl glycerol dibiphytanyl glycerol tetraether; 3. monoglycosyl-phosphatidylglycerol glycerol dibiphytanyl glycerol tetraether; 4. Monoglycosyl archaeol; 5. diglycosyl archaeol; 6. phosphatidylethanolamine archaeol; 7. 1,2-dihexarachidoyl-sn-glycero-3-phosphatidylcholine (PC), DAG=diacylglycerol, AEG=acyletherglycerol, DEG=dietherglycerol; 8. D-glucosyl-1,1'-N-stearoyl-D-erythro-sphingosine, PI=phosphatidylinositol; 9. 1,2-dipalmitoyl-sn-glycero-3-O-4'-(N,N,N-trimethyl)-homoserine, BL=betaine lipids, OL=ornithine lipids; 10. 1,2-dipalmitoyl-sn-glycero-3-phosphatidylethanolamine (PE); 11. 1,2-dipalmitoyl-sn-glycero-3-phosphoethanolamine-N,N-dimethyl (PDME), PME=phosphatidylmethylethanolamine; 12. 1',3'-bis[1,2-dioleoyl-sn-glycero-3-phospho]-sn-glycerol or cardiolipin (CL); 13. 1,2-dipalmitoyl-sn-glycero-3-phospho-(1'-rac-glycerol). *archaeols included AR, OH-AR, 2OH-AR and Ext-OH-AR (for abbreviations of archaeal lipids please see Table SXX).

Table S2. Compilation of raw lipid data for this study (both the IPL (bacteria & archaea) and ASL (archaeal-specific IPL & core lipid) datasets).

Supplementary Table 2 can be found in .xlsx format in the Caltech online repository along with this thesis.

Table S3. Possible sources of archaeal polar lipids in carbonates according to Rossel et al. (2011), Yoshinaga et al. (2015), and Kellermann et al. (2016).

Polar Lipids*	Potential Source
G-GDGT(0-5)	ANME-1, Thaumarchaeota GDGT(5)
2G-GDGT(0-5)	ANME-1, Thaumarchaeota GDGT(5)
PG-GDGT(0-4)-G/2G/PG	ANME-1
G/2G-AR/OH-AR	ANME-1 (AR), ANME-2 (AR+OH-AR)
PE-AR/OH-AR	ANME-1? (see Wegener et al., 2016)
PG/PI/PE/PS-AR/OH-AR	ANME-1 (AR), ANME-2 (AR+OH-AR)
PG/PS-2OH-AR	ANME-2
PI-Ext-OH-AR	ANME-2

*G=monoglycosyl; 2G=diglycosyl; PG=phosphatidylglycerol;
 PI=phosphatidylinositol; PS=phosphatidylserine;
 PE=phosphatidylethanolamine; GDGT=glycerol-dibiphytanyl-glycerol-
 tetraether (note that the numbers in parenthesis correspond to numbers of
 rings, being 5 the crenarchaeol); AR=archaeol; OH-AR=hydroxylated AR;
 2OH-AR=dihydroxylated AR; Ext-OH-AR=extended (C₂₅-C₂₀) OH-AR.

Table S4. Table listing Pearson R values for correlations between 16S rRNA gene OTUs and each of the lipids from the IPL and ASL datasets. Values are only given if the Pearson R value is >0.8 and the p-value is <0.05 . Correlations were determined from all native-active and native-low-activity carbonates.

Supplementary Table 4 can be found in .xlsx format in the Caltech online repository along with this thesis.

Table S5. Biomarker data used to generate Venn diagrams in this study (Fig. 5; Fig. S1).

Supplementary Table 5 can be found in .xlsx format in the Caltech online repository along with this thesis.

3.11 SUPPLEMENTAL MATERIAL: FIGURES

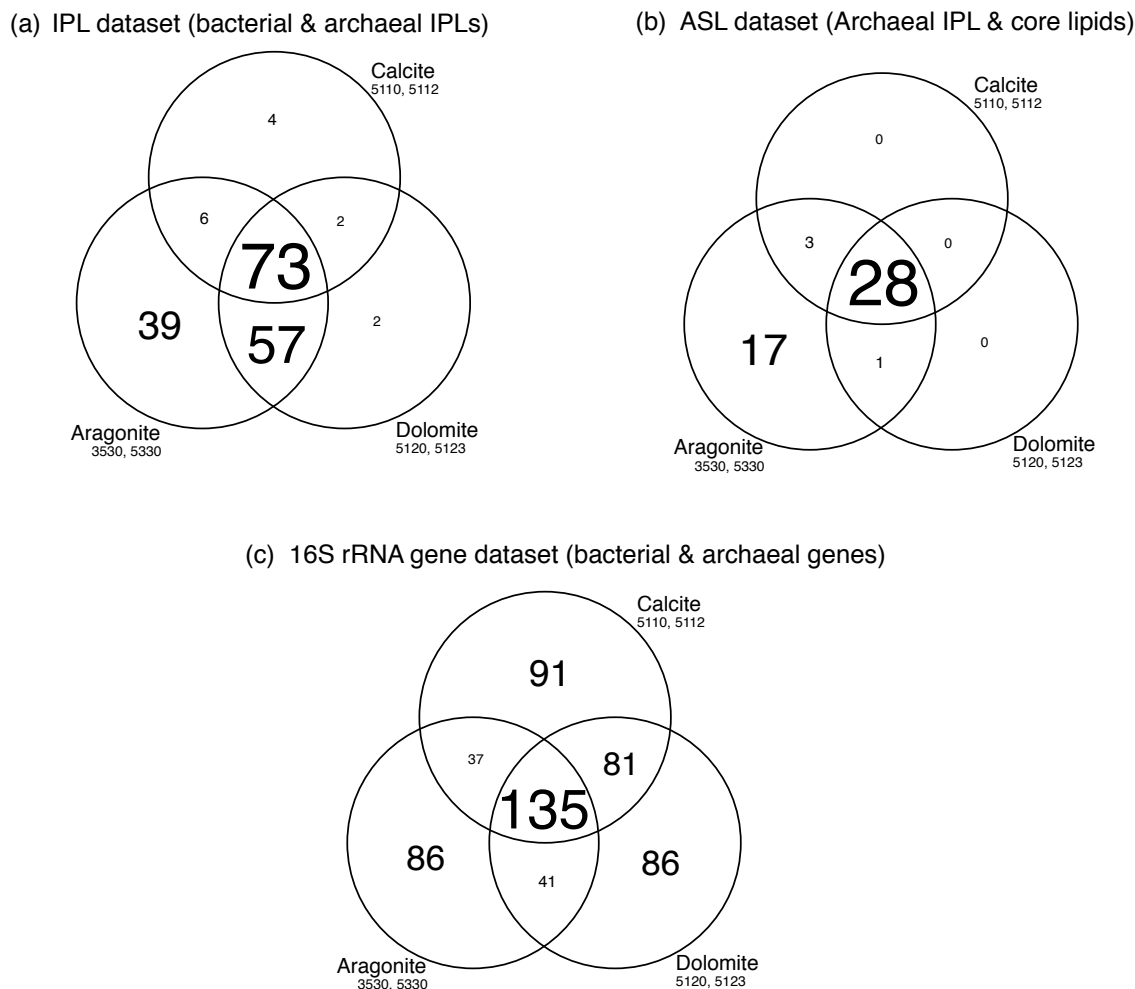


Fig. S1: Venn diagrams of the (a) IPL, (b) ASL, and (c) 16S rRNA gene datasets, binned by mineralogy. In order to avoid sample bias for any particular mineralogy, two carbonates were chosen to represent each of aragonite, calcite, and dolomite from the set of native-active carbonates. Only native carbonates from active seep sites were considered in order to remove seep activity as a factor affecting taxa distribution. The two carbonates with highest proportions of each morphology were chosen, based on XRD data. In order for a biomarker to count as “present” for this presence/absences analysis, it must have been observed in both replicates. In each field of the Venn diagrams, text size is proportional to value to help guide the readers’ eye. The two IPLs in (a) identified as diagnostic of dolomite are bacterial: C65:3 cardiolipin-DAG and C31:0 PE-DAG.

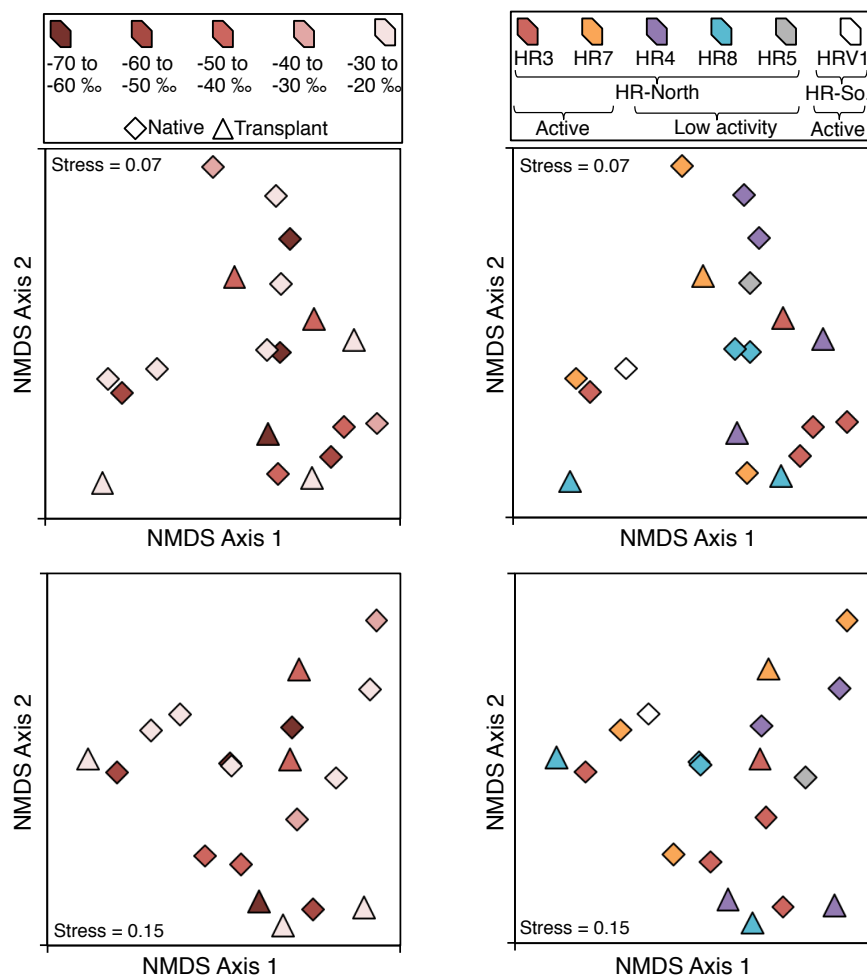


Fig S2: NMDS ordination of IPL relative abundance data. (a,c) Samples grouped by $\delta^{13}\text{C}_{\text{org}}$ value, (b,d) samples grouped by seafloor station. (a,b) Absolute abundance profiles of the IPL dataset. (c,d) Relative abundance profiles of the IPL data set. Neither $\delta^{13}\text{C}_{\text{org}}$ nor seafloor station significantly differentiate the lipid profiles.

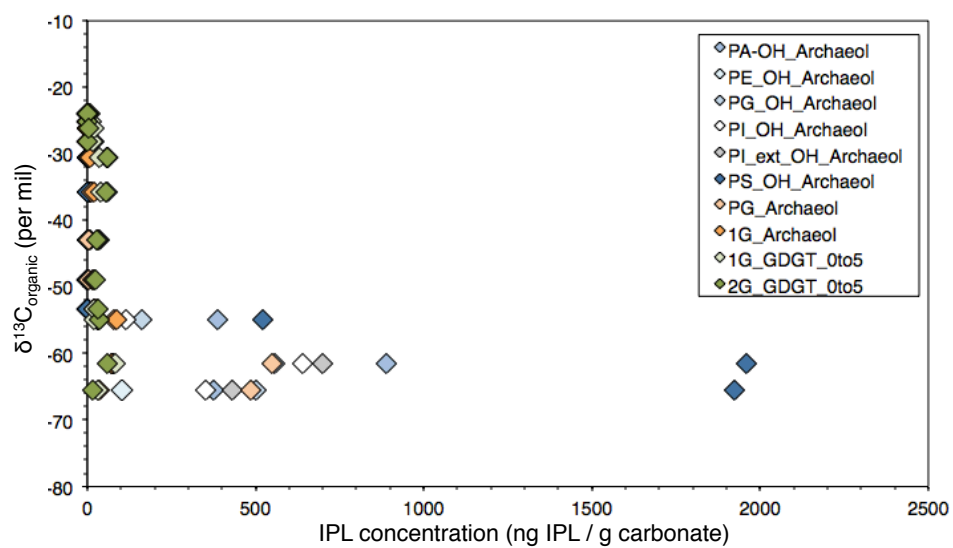


Fig. S3: Cross-plot of $\delta^{13}\text{C}_{\text{org}}$ vs concentration of various archaeal IPLs. Samples with the highest concentrations of OH-AR also exhibit the most depleted $\delta^{13}\text{C}_{\text{org}}$ values.

3.12 REFERENCES

- Aloisi, G., I. Bouloubassi, S. K. Heijs, R. D. Pancost, C. Pierre, J. S. Sinninghe Damsté, J. C. Gottschal, L. J. Forney, and J.-M. Rouchy. 2002. CH₄-consuming microorganisms and the formation of carbonate crusts at cold seeps. *Earth and Planetary Science Letters* **203**: 195–203.
- Bayon, G., G. M. Henderson, and M. Bohn. 2009. U–Th stratigraphy of a cold seep carbonate crust. *Chemical Geology* **260**: 47–56.
- Benincà, E., J. Huisman, R. Heerkloss, K. D. Jöhnk, P. Branco, E. H. Van Nes, M. Scheffer, and S. P. Ellner. 2008. Chaos in a long-term experiment with a plankton community. *Nature* **451**: 822–825.
- Bergmann, K. 2013. Constraints on the carbon cycle and climate during the early evolution of animals.
- Berner, R. A. 1980. *Earth Diagenesis*, Princeton University Press.
- Birgel, D., D. Feng, H. H. Roberts, and J. Peckmann. 2011. Changing redox conditions at cold seeps as revealed by authigenic carbonates from Alaminos Canyon, northern Gulf of Mexico. *Chemical Geology* **285**: 82–96.
- Birgel, D., J. Peckmann, S. Klautzsch, V. Thiel, and J. Reitner. 2006a. Anaerobic and Aerobic Oxidation of Methane at Late Cretaceous Seeps in the Western Interior Seaway, USA. *Geomicrobiology Journal* **23**: 565–577.
- Birgel, D., M. Elvert, X. Han, and J. Peckmann. 2008a. ¹³C-depleted biphytanic diacids as tracers of past anaerobic oxidation of methane. *Organic geochemistry* **39**: 152–156.
- Birgel, D., T. Himmler, A. Freiwald, and J. Peckmann. 2008b. A new constraint on the antiquity of anaerobic oxidation of methane: Late Pennsylvanian seep limestones from southern Namibia. *Geology* **36**: 543–546.
- Birgel, D., V. Thiel, Hinrichs, M. Elvert, K. A. Campbell, J. Reitner, J. D. Farmer, and J. Peckmann. 2006b. Lipid biomarker patterns of methane-seep microbialites from the Mesozoic convergent margin of California. *Organic geochemistry* **37**: 1289–1302.
- Blättler, C.L., N.R. Miller, and J.A. Higgins. 2015. Mg and Ca isotope signatures of authigenic dolomite in siliceous deep-sea sediments. *Earth and Planetary Science Letters* **419**: 32–42. doi:10.1016/j.epsl.2015.03.006.
- Blumenberg, M., E.-O. Walliser, M. Taviani, R. Seifert, and J. Reitner. 2015. Authigenic carbonate formation and its impact on the biomarker inventory at hydrocarbon seeps – A case study from the Holocene Black Sea and the Plio-Pleistocene Northern Apennines (Italy). *Marine and Petroleum Geology* **66**: 532–541.
- Blumenberg, M., R. Seifert, J. Reitner, T. Pape, and W. Michaelis. 2004. Membrane lipid patterns typify distinct anaerobic methanotrophic consortia. *Proceedings of the National Academy of Sciences* **101**: 11111–11116.
- Boetius, A., and E. Suess. 2004. Hydrate Ridge: a natural laboratory for the study of microbial life fueled by methane from near-surface gas hydrates. *Chemical Geology* **205**: 291–310.
- Boetius, A., K. Ravensschlag, C. J. Schubert, D. Rickert, F. Widdel, A. Gieseke, R. Amann, B. B. Jørgensen, U. Witte, and O. Pfannkuche. 2000. A marine microbial consortium apparently mediating anaerobic oxidation of methane. *Nature* **407**: 623–626.
- Bristow, T.F., M. Bonifacie, A. Derkowski, J.M. Eiler, and J.P. Grotzinger. 2011. A hydrothermal origin for isotopically anomalous cap dolostone cements from south China. *Nature* **474**: 68–71. doi:10.1038/nature10096.
- Burton, E. A. 1993. Controls on marine carbonate cement mineralogy: review and reassessment. *Chemical Geology* **105**: 163–179.
- Case, D. H., A. L. Pasulka, J. J. Marlow, B. M. Grupe, L. A. Levin, and V. J. Orphan. 2015.

- Methane Seep Carbonates Host Distinct, Diverse, and Dynamic Microbial Assemblages. *mBio* **6**: e01348–15.
- Dell'Anno, A., M. Fabiano, G. C. A. Duineveld, A. Kok, and R. Danovaro. 1998. Nucleic Acid (DNA, RNA) Quantification and RNA/DNA Ratio Determination in Marine Sediments: Comparison of Spectrophotometric, Fluorometric, and HighPerformance Liquid Chromatography Methods and Estimation of Detrital DNA. *Applied and Environmental Microbiology* **64**: 3238–3245.
- Elvert, M., A. Boetius, K. Knittel, and B. B. Jørgensen. 2003. Characterization of Specific Membrane Fatty Acids as Chemotaxonomic Markers for Sulfate-Reducing Bacteria Involved in Anaerobic Oxidation of Methane. *Geomicrobiology Journal* **20**: 403–419.
- Faust, K., L. Lahti, D. Gonze, W. M. de Vos, and J. Raes. 2015. Metagenomics meets time series analysis: unraveling microbial community dynamics. *Current Opinion in Microbiology* **25**: 56–66.
- Gieskes, J., C. Mahn, S. Day, J. Martin, J. Greinert, T. Rathburn, and B. McAdoo. 2005. A study of the chemistry of pore fluids and authigenic carbonates in methane seep environments: Kodiak Trench, Hydrate Ridge, Monterey Bay, and Eel River Basin. *Chemical Geology* **220**: 329–345.
- Goedert, J. L., V. Thiel, O. Schmale, W. W. Rau, W. Michaelis, and J. Peckmann. 2003. The Late Eocene “Whiskey Creek” methane-seep deposit (western Washington State). *Facies* **48**: 223–239.
- Greinert, J., G. Bohrmann, and E. Suess. 2001. Gas Hydrate-Associated Carbonates and Methane-Venting at Hydrate Ridge: Classification, Distribution, and Origin of Authigenic Lithologies, p. 99–113. *In* C.K. Paull and W.P. Dillon [eds.], *Natural Gas Hydrates*. American Geophysical Union.
- Hagemann, A., T. Leefmann, J. Peckmann, V.-E. Hoffmann, and V. Thiel. 2012. Biomarkers from individual carbonate phases of an Oligocene cold-seep deposit, Washington State, USA. *Lethaia* **46**: 7–18.
- Heijs, S. K., G. Aloisi, I. Bouloubassi, R. D. Pancost, C. Pierre, J. S. Sinninghe Damsté, J. C. Gottschal, J. D. Elsas, and L. J. Forney. 2006. Microbial Community Structure in Three Deep-Sea Carbonate Crusts. *Microbial Ecology* **52**: 451–462.
- Hinrichs. 2002. Microbial fixation of methane carbon at 2.7 Ga: Was an anaerobic mechanism possible? *Geochemistry Geophysics Geosystems* **3**: 1042.
- Hinrichs, R. E. Summons, V. Orphan, S. P. Sylva, and J. M. Hayes. 2000. Molecular and isotopic analysis of anaerobic methane-oxidizing communities in marine sediments. *Organic Geochemistry* **31**: 1685–1701.
- Hoffmann-Sell, L., D. Birgel, E. T. Arning, K. B. Föllmi, and J. Peckmann. 2011. Archaeal lipids in Neogene dolomites (Monterey and Sisquoc Formations, California) – Planktic versus benthic archaeal sources. *Organic geochemistry* **42**: 593–604.
- Jiang, G., M. J. Kennedy, and N. Christie-Blick. 2003. Stable isotopic evidence for methane seeps in Neoproterozoic postglacial cap carbonates. *Nature* **426**: 822–826.
- Katz, M. E., D. K. Pak, G. R. Dickens, and K. G. Miller. 1999. The Source and Fate of Massive Carbon Input During the Latest Paleocene Thermal Maximum. *Science* **286**: 1531–1533.
- Kellermann, M. Y., M. Y. Yoshinaga, G. Wegener, V. Krukenberg, and Hinrichs. 2016. Tracing the production and fate of individual archaeal intact polar lipids using stable isotope probing. *Organic geochemistry* **95**: 13–20.
- Kiel, S., D. Birgel, K. A. Campbell, J. S. Crampton, P. Schiøler, and J. Peckmann. 2013. Cretaceous methane-seep deposits from New Zealand and their fauna. *Palaeogeography, Palaeoclimatology, Palaeoecology* **390**: 17–34.
- Knittel, K., T. Lösekann, A. Boetius, R. Kort, and R. Amann. 2005. Diversity and Distribution of Methanotrophic Archaea at Cold Seeps. *Applied and Environmental Microbiology* **71**: 467–479.

- Korhonen, J., J. Soininen, and H. Hillebrand. 2010. A quantitative analysis of tempoeral turnover in aquatic species assemblages across ecosystems. *Ecology* **91**: 508–517.
- Kulm, L. D., and E. Suess. 1990. Relationship between carbonate deposits and fluid venting: Oregon Accretionary Prism. *Journal of Geophysical Research: Solid Earth* **95**: 8899–8915.
- Leefmann, T., J. Bauermeister, A. Kronz, V. Liebetrau, J. Reitner, and V. Thiel. 2008. Miniaturized biosignature analysis reveals implications for the formation of cold seep carbonates at Hydrate Ridge (off Oregon, USA). *Biogeosciences* **5**: 731–738.
- Levin, L. A., G. F. Mendoza, J. P. Gonzalez, A. R. Thurber, and E. E. Cordes. 2010. Diversity of bathyal macrofauna on the northeastern Pacific margin: the influence of methane seeps and oxygen minimum zones. *Marine Ecology Progress Series* **31**: 94–110.
- Levy-Booth, D. J., R. G. Campbell, and R. H. Gulden. 2007. Cycling of extracellular DNA in the soil environment. *Soil Biology & Biochemistry* **39**: 2977–2991.
- Lipp, J. S., Y. Morono, F. Inagaki, and Hinrichs. 2008. Significant contribution of Archaea to extant biomass in marine subsurface sediments. *Nature* **454**: 991–994.
- Little, C. T. S., D. Birgel, A. J. Boyce, J. A. Crame, J. E. Francis, S. Kiel, J. Peckmann, D. Pirrie, G. K. Rollinson, and J. D. Witts. 2015. Late Cretaceous (Maastrichtian) shallow water hydrocarbon seeps from Snow Hill and Seymour Islands, James Ross Basin, Antarctica. *Palaeogeography, Palaeoclimatology, Palaeoecology* **418**: 213–228.
- Lloyd, K.G., D.B. Albert, J.F. Biddle, J.P. Chanton, O. Pizarro, and A. Teske. 2010. Spatial Structure and Activity of Sedimentary Microbial Communities Underlying a *Beggiatoa* spp. Mat in the Gulf of Mexico Hydrocarbon Seep. *PLoS ONE* **5**: e8737. doi:10.1371/journal.pone.0008738.
- Logemann, J., J. Graue, J. Köster, B. Engelen, J. Rullkötter, and H. Cypionka. 2011. A laboratory experiment of intact polar lipid degradation in sandy sediments. *Biogeosciences* **8**: 2547–2560.
- Luff, R., K. Wallmann, and G. Aloisi. 2004. Numerical modeling of carbonate crust formation at cold vent sites: significance for fluid and methane budgets and chemosynthetic biological communities. *Earth and Planetary Science Letters* **221**: 337–353.
- Marlow, J. J., J. A. Steele, W. Ziebis, A. R. Thurber, L. A. Levin, and V. J. Orphan. 2014a. Carbonate-hosted methanotrophy represents an unrecognized methane sink in the deep sea. *Nature Communications* **5**: 1–12.
- Marlow, J., J. A. Steele, D. Case, S. A. Connon, L. A. Levin, and V. J. Orphan. 2014b. Microbial abundance and diversity patterns associated with sediments and carbonates from the methane seep environments of Hydrate Ridge, OR. *Frontiers in Marine Science* **1**: 1–16.
- Meador, T. B., E. J. Gagen, M. E. Loscar, and T. Goldhammer. 2014. *Thermococcus kodakarensis* modulates its polar membrane lipids and elemental composition according to growth stage and phosphate availability. *Frontiers in Microbiology* **5**: 1–13.
- Moore, J. C., D. Orange, and L. D. Kulm. 1990. Interrelationship of fluid venting and structural evolution: Alvin observations from the frontal accretionary prism, Oregon. *Journal of Geophysical Research: Solid Earth* **95**: 8795–8808.
- Naehr, T.H., P. Eichhubl, V.J. Orphan, M. Hovland, C.K. Paull, W. Ussler III, T.D. Lorenson, and H.G. Greene. 2007. Authigenic carbonate formation at hydrocarbon seeps in continental margin sediments: A comparative study. *Deep-Sea Research II* **54**: 1268–1291. doi:10.1016/j.dsr2.2007.04.010.
- Natalicchio, M., J. Peckmann, D. Birgel, and S. Kiel. 2015. Seep deposits from northern Istria, Croatia: a first glimpse into the Eocene seep fauna of the Tethys region. *Geol. Mag.* **152**: 444–459.
- Niemann, H., and M. Elvert. 2008. Diagnostic lipid biomarker and stable carbon isotope signatures of microbial communities mediating the anaerobic oxidation of methane with sulphate. *Organic geochemistry* **39**: 1668–1677.
- Oksanen, J., F. G. Blanchet, R. Kindt, P. Legendre, P. Minchin, R. B. OHara, G. Simpson, P.

- Solymos, M. H. H. Stevens, and H. Wagner. 2013. *vegan*: Community Ecology Package.
- Orphan, V. J., Hinrichs, W. Ussler, C. K. Paull, L. T. Taylor, S. P. Sylva, J. M. Hayes, and E. F. Delong. 2001. Comparative Analysis of Methane-Oxidizing Archaea and Sulfate-Reducing Bacteria in Anoxic Marine Sediments. *Applied and Environmental Microbiology* **67**: 1922–1934.
- Orphan, V., W. Ussler, T. H. Naehr, C. H. House, Hinrichs, and C. K. Paull. 2004. Geological, geochemical, and microbiological heterogeneity of the seafloor around methane vents in the Eel River Basin, offshore California. *Chemical Geology* **205**: 265–289.
- Pancost, R. D., I. Bouloubassi, G. Aloisi, J. S. Sinninghe Damsté, and T. M. S. Scientific Party. 2001. Three series of non-isoprenoidal dialkyl glycerol diethers in cold-seep carbonate crusts. *Organic geochemistry* **32**: 695–707.
- Pasulka, A. L., L. A. Levin, J. A. Steele, D. H. Case, M. R. Landry, and V. J. Orphan. 2015. Microbial eukaryotic distributions and diversity patterns in a deep-sea methane seep ecosystem. *Environmental microbiology* doi:10.1111/1462-2920.13185.
- Pearson, A., S. J. Hurley, S. R. S. Walter, S. Kusch, S. Lichtin, and Y. G. Zhang. 2016. Stable carbon isotope ratios of intact GDGTs indicate heterogeneous sources to marine sediments. *Geochimica et Cosmochimica Acta* **181**: 18–35.
- Peckmann, J., and J. L. Goedert. 2005. Geobiology of ancient and modern methane-seeps. *Palaeogeography, Palaeoclimatology, Palaeoecology* **227**: 1–5.
- Peckmann, J., D. Birgel, and S. Kiel. 2009. Molecular fossils reveal fluid composition and flow intensity at a Cretaceous seep. *Geology* **37**: 847–850.
- Peckmann, J., J. L. Goedert, V. Thiel, W. Michaelis, and J. Reitner. 2002. A comprehensive approach to the study of methane-seep deposits from the Lincoln Creek Formation, western Washington State, USA. *Sedimentology* **49**: 855–873.
- Peckmann, J., V. Thiel, W. Michaelis, P. Clari, C. Gaillard, L. Martire, and J. Reitner. 1999. Cold seep deposits of Beauvoisin (Oxfordian; southeastern France) and Marmorito (Miocene; northern Italy): microbially induced authigenic carbonates. *Int J Earth Sci (Geol Rundsch)* **88**: 60–75.
- Pop Ristova, P., F. Wenzhöfer, A. Ramette, J. Felden, and A. Boetius. 2015. Spatial scales of bacterial community diversity at cold seeps (Eastern Mediterranean Sea). *The ISME Journal* **9**: 1306–1318.
- R Core Team. 2014. *R*: A language and environment for statistical computing.
- Rasmussen, B. 2000. Filamentous microfossils in a 3,235-million-year-old volcanogenic massive sulphide deposit. *Nature* **405**: 676–679.
- Reeburgh, W. S. 2007. Oceanic Methane Biogeochemistry. *Chemical Reviews* **107**: 486–513.
- Reitner, J., J. Peckmann, A. Reimer, G. Schumann, and V. Thiel. 2005. Methane-derived carbonate build-ups and associated microbial communities at cold seeps on the lower Crimean shelf (Black Sea). *Facies* **51**: 66–79.
- Ritger, S., B. Carson, and E. Suess. 1987. Methane-derived authigenic carbonates formed by subduction-induced pore-water expulsion along the Oregon/Washington margin. *Geological Society of America Bulletin* **98**: 147–156.
- Rossel, P. E., J. S. Lipp, H. F. Fredricks, J. Arnds, A. Boetius, M. Elvert, and Hinrichs. 2008. Intact polar lipids of anaerobic methanotrophic archaea and associated bacteria. *Organic geochemistry* **39**: 992–999.
- Rossel, P. E., M. Elvert, A. Ramette, A. Boetius, and Hinrichs. 2011. Factors controlling the distribution of anaerobic methanotrophic communities in marine environments: Evidence from intact polar membrane lipids. *Geochimica et Cosmochimica Acta* **75**: 164–184.
- Ruff, S. E., J. F. Biddle, A. P. Teske, K. Knittel, A. Boetius, and A. Ramette. 2015. Global dispersion and local diversification of the methane seep microbiome. *Proceedings of the National Academy of Sciences* 1–6.
- Rütters, H., H. Sass, H. Cypionka, and J. Rullkötter. 2001. Monoalkylether phospholipids in the

- sulfate-reducing bacteria *Desulfosarcina variabilis* and *Desulforhabdus amnigenus*. *Archives of microbiology* **176**: 435–442.
- Sahling, H., D. Rickert, R. W. Lee, P. Linke, and E. Suess. 2002. Macrofaunal community structure and sulfide flux at gas hydrate deposits from the Cascadia convergent margin, NE Pacific. *Marine Ecology Progress Series* **231**: 121–138.
- Schrag, D. P., J. A. Higgins, F. A. Macdonald, and D. T. Johnston. 2013. Authigenic Carbonate and the History of the Global Carbon Cycle. *Science* **339**: 540–543.
- Schubotz, F., J. S. Lipp, M. Elvert, and Hinrichs. 2011. Stable carbon isotopic compositions of intact polar lipids reveal complex carbon flow patterns among hydrocarbon degrading microbial communities at the Chapopote asphalt volcano. *Geochimica et Cosmochimica Acta* **75**: 4399–4415.
- Shade, A., J. G. Caporaso, J. Handelsman, R. Knight, and N. Fierer. 2013. A meta-analysis of changes in bacterial and archaeal communities with time. *The ISME Journal* **7**: 1493–1506.
- Simon, M., and F. Azam. 1989. Protein content and protein synthesis rates of planktonic marine bacteria. *Marine ecology progress series* **51**: 201–213.
- Slotznick, S.P., and W.W. Fischer. 2016. Examining Archean methanotrophy. *Earth and Planetary Science Letters* **441**: 52–59. doi:10.1016/j.epsl.2016.02.013.
- Stadnitskaia, A., D. Nadezhkin, B. Abbas, V. Blinova, M. K. Ivanov, and J. S. Sinninghe Damsté. 2008. Carbonate formation by anaerobic oxidation of methane: Evidence from lipid biomarker and fossil 16S rDNA. *Geochimica et Cosmochimica Acta* **72**: 1824–1836.
- Sturt, H. F., R. E. Summons, K. Smith, M. Elvert, and Hinrichs. 2004. Intact polar membrane lipids in prokaryotes and sediments deciphered by high-performance liquid chromatography/electrospray ionization multistage mass spectrometry—new biomarkers for biogeochemistry and microbial ecology. *Rapid Commun. Mass Spectrom.* **18**: 617–628.
- Suess, E., B. Carson, S. D. Ritger, J. C. Moore, M. L. Jones, L. D. Kulm, and G. R. Cochrane. 1985. Biological communities at vent sites along the subduction zone off Oregon. *Bulletin of the Biological Society of Washington* **6**: 475–484.
- Teichert, B., A. Eisenhauer, G. Bohrmann, A. Haase-Schramm, B. Bock, and P. Linke. 2003. U/Th systematics and ages of authigenic carbonates from Hydrate Ridge, Cascadia Margin: Records of fluid flow variations. *Geochimica et Cosmochimica Acta* **67**: 3845–3857.
- Teichert, B., G. Bohrmann, and E. Suess. 2005. Chemoherms on Hydrate Ridge—Unique microbially-mediated carbonate build-ups growing into the water column. *Palaeogeography, Palaeoclimatology, Palaeoecology* **227**: 67–85.
- Tennant, C. B., and R. W. Berger. 1957. X-ray determination of dolomite-calcite ratio of a carbonate rock. *American Mineralogist* **42**: 23–29.
- Thiel, V., J. Peckmann, R. Seifert, P. Wehrung, J. Reitner, and W. Michaelis. 1999. Highly isotopically depleted isoprenoids: molecular markers for ancient methane venting. *Geochimica et Cosmochimica Acta* **63**: 3959–3966.
- Torti, A., M. A. Lever, and B. B. Jørgensen. 2015. Origin, dynamics, and implications of extracellular DNA pools in marine sediments. *Marine Genomics* **24**: 185–196.
- Trembath-Reichert, E., D. H. Case, and V. J. Orphan. 2016. Characterization of microbial associations with methanotrophic archaea and sulfate-reducing bacteria through statistical comparison of nested Magneto-FISH enrichments. *PeerJ* **4**: e1913–31.
- Treude, T., A. Boetius, K. Knittel, K. Wallmann, and B. B. Jørgensen. 2003. Anaerobic oxidation of methane above gas hydrates at Hydrate Ridge, NE Pacific Ocean. *Marine Ecology Progress Series* **264**: 1–14.
- Tryon, M. D., K. M. Brown, and M. E. Torres. 2002. Fluid and chemical flux in and out of sediments hosting methane hydrate deposits on Hydrate Ridge, OR, II: Hydrological processes. *Earth and Planetary Science Letters* **201**: 541–557.
- Tryon, M. D., K. M. Brown, M. E. Torres, A. M. Tréhu, J. McManus, and R. W. Collier. 1999. Measurements of transience and downward fluid flow near episodic methane gas vents,

- Hydrate Ridge, Cascadia. *Geology* **27**: 1075–1078.
- Van Lith, Y., R. Warthmann, C. Vasconcelos, and J. A. Mckenzie. 2003. Microbial fossilization in carbonate sediments: a result of the bacterial surface involvement in dolomite precipitation. *Sedimentology* **50**: 237–245.
- Vasconcelos, C., J. A. Mckenzie, S. Bernasconi, D. Grujic, and A. J. Tiens. 1995. Microbial mediation as a possible mechanism for natural dolomite formation at low temperatures. *Nature* **377**: 220–222.
- Warthmann, R., C. Vasconcelos, H. Sass, and J. A. Mckenzie. 2005. *Desulfovibrio brasiliensis* sp. nov., a moderate halophilic sulfate-reducing bacterium from Lagoa Vermelha (Brazil) mediating dolomite formation. *Extremophiles* **9**: 255–261.
- Wegener, G., and A. Boetius. 2009. Short-term changes in anaerobic oxidation of methane in response to varying methane and sulfate fluxes. *Biogeosciences* **6**: 867–876.
- White, D., D. B. Ringelberg, S. J. Macnaughton, S. Alugupalli, and D. Schram. 1997. Signature Lipid Biomarker Analysis for Quantitative Assessment In Situ of Environmental Microbial Ecology, p. 22–34. *In* R.P. Eganhouse [ed.], *Molecular Markers in Environmental Geochemistry*. American Chemical Society.
- White, D., W. Davis, J. Nickels, J. King, and R. Bobbie. 1979. Determination of the sedimentary microbial biomass by extractible lipid phosphate. *Oecologia* **40**: 51–62.
- Wörmer, L., J. S. Lipp, J. M. Schröder, and Hinrichs. 2013. Application of two new LC–ESI–MS methods for improved detection of intact polar lipids (IPLs) in environmental samples. *Organic geochemistry* **59**: 10–21.
- Xie, S., J. S. Lipp, G. Wegener, T. G. Ferdelman, and Hinrichs. 2013. Turnover of microbial lipids in the deep biosphere and growth of benthic archaeal populations. *Proceedings of the National Academy of Sciences* **110**: 6010–6014.
- Yoshinaga, M. Y., C. S. Lazar, M. Elvert, Y.-S. Lin, C. Zhu, V. B. Heuer, A. Teske, and Hinrichs. 2015. Possible roles of uncultured archaea in carbon cycling in methane-seep sediments. *Geochimica et Cosmochimica Acta* **164**: 35–52.
- Yoshinaga, M. Y., M. Y. Kellermann, P. E. Rossel, F. Schubotz, J. S. Lipp, and Hinrichs. 2011. Systematic fragmentation patterns of archaeal intact polar lipids by high-performance liquid chromatography/electrospray ionization ion-trap mass spectrometry. *Rapid Commun. Mass Spectrom.* **25**: 3563–3574.
- Zink, K.-G., H. Wilkes, U. Disko, M. Elvert, and B. Horsfield. 2003. Intact phospholipids—microbial “life markers” in marine deep subsurface sediments. *Organic geochemistry* **34**: 755–769.
- Zink, K.-G., K. Mangelsdorf, L. Granina, and B. Horsfield. 2008. Estimation of bacterial biomass in subsurface sediments by quantifying intact membrane phospholipids. *Anal Bioanal Chem* **390**: 885–896.

